1st Technical Design Report

for the Seeding @ SPARC experiment

27 June 2005

Seeding @ SPARC logo

Contributors

L. Poletto, G. Tondello
Istituto Nazionale per la Fisica della Materia (INFM) LUXOR - Laboratory for UV and X-Ray Optical Research c/o Department of Information Engineering via Gradenigo 6/B 35131 Padova (Italy)

S. De Silvestri, M. Nisoli, S. Stagira
Politecnico di Milano, piazza L. Da Vinci, 32 - 20133 Milano (Italy)

P. Musumeci, M. Petrarca
Università di Roma "La Sapienza" P. Le Aldo Moro 65 (Italy)

M.E. Couprie, G. Lambert, H. Merdji, P. Breger, D. Garzella, J.F. Hergott, P. Monchicourt, P. Salières, B. Carré.
Service des Photons Atomes et Molécules, CEA Saclay, DSM/DRECAM, bât 522, 91 191 Gif-sur-Yvette (France)

D. Alesini, M. Biagini, A. Clozza, G. Di Pirro, A. Drago, M. Ferrario, V. Fusco, S. Gallo, A. Ghigo, V. Lollo, M. Migliorati, L. Palumbo, L. Pellegrino, C. Sanelli, F. Sgamma, B. Spataro, C. Vaccarezza, C. Vicario
INFN – LNF, Via E. Fermi, 44, 00044 Frascati (Italy)

L. Serafini
INFN-Milan and University of Milan Department of Physics Via Celoria 16 , 20133 Milano (Italy)

M. Carpanese, F. Ciocci, G. Dattoli, A. Dipace, A. Doria, G. P. Gallerano, L. Giannessi, E. Giovenale, P. L. Ottaviani, G. Parisi, I. Spassovsky, M. Quattromini, S. Pagnutti, A. Renieri, C. Ronsivalle, E. Sabia, S. Spampanati, E. Campana, G. Ronci, M. Sassi
ENEA C.R. Frascati, Via E. Fermi 45, 00044 Frascati (Italy)

Edited by L. Giannessi

Acknowledgments - *This work has been partially funded by the EU under the 6th Framework programme, contract no. 011935 EUROFEL*

Index

Abstract

The future development of linac-based FEL sources producing short wavelength radiation offers unique opportunities in different scientific domains. The Self Amplified Spontaneous Emission (SASE) scheme has been demonstrated as an efficient way to obtain radiation in such spectral range, but it requires very long insertion devices to achieve saturation and the light delivered is not fully temporally coherent.

When the FEL is operated as an amplifier of an external seed signal, the coherence properties are determined by the seed and FEL radiation has significantly lower intensity fluctuations. The harmonic generation process in an FEL can be exploited to widen the wavelength range of operation toward the shorter wavelengths. The two concepts, of seeding and harmonic generation, can be merged in a single device which can provide both temporally and spatially coherent radiation at short wavelengths, with significantly reduced intensity fluctuations and in a more compact and less expensive configuration.

High order harmonics generated in gas by high power Ti:Sa laser pulses represent promising candidates as seed sources for FELs for several reasons, as spatial and temporal coherence, wavelength tunability and spectral range, which extends down to the nanometre wavelength scale.

This document describes a research work plan that will be implemented at the SPARC FEL facility with the main goal of studying the amplification and the harmonic generation processes of an input seed signal obtained as higher order harmonics generated both in crystal (400 nm and 266 nm) and in gas (266 nm, 160 nm, 114 nm) from a high intensity Ti:Sa laser pulse.

1. Introduction

1.1. Seeded Free Electron Lasers

During the last years, new schemes other than the Self Amplified Spontaneous Emission (*SASE*) have been proposed for reaching very short wavelengths in systems based on Free Electron Laser (FEL) [1][2][3][4], where the main goal is to have more compact and fully temporally coherent sources. The idea of operating a Free Electron Laser from a pre-bunched electron beam traces back to the late 80's when an oscillator-based FEL resonating at 240 nm was proposed for seeding a single pass FEL amplifier operating at 80 nm with the same e-beam [5]. More recent proposals foresee self-seeding as a mean to improve the radiation brightness by reducing the spectral line-width of the SASE source (DESY [6]). Seeded FEL amplifier operation in combination with harmonic generation has been demonstrated experimentally in Brookhaven [3]. In this arrangement, an external laser source is seeded into a modulator, i.e. an undulator where a periodic energy modulation is induced in the electron beam. This modulation occurs with the periodicity of the seed wavelength, the successive beam evolution in a dispersive section induces the conversion of the energy modulation into a density modulation and consistent emission of radiation at higher order harmonics with longitudinal and transverse coherence reproducing those of the laser seed. The idea of seeding or self-seeding an FEL amplifier and then using the induced energy/phase modulation in order to produce radiation at the harmonics of the fundamental in a cascaded FEL configuration is quite widespread, and plays a significant role in many of the existing or proposed FEL projects in Europe, as listed in Tab. I ([6][7][8][9][10][11][12][13][14]).

Tab. I. *List of existing or proposed facilities planning seeding and/or harmonic generation in Europe (HHG = High-order Harmonics generated in Gas, NLC =Non Linear Crystal)*

Project name	Wavelength range (nm)	Scheme
4GLS	IR – XUV	Seeding
ARC-EN-CIEL	200 – 0.82	Seeding from HHG
BESSY	51 – 1	Seeding
TTF – TESLA FEL	6 – 0.082	Self-seeding
FERMI (ELETTRA)	100 – 40	Seeding
MAX – 4	260 – 10	Seeding from NLC
SPARX	15 – 1.5	Seeding from HHG
SCSS	80 – 40	Seeding from HHG

These proposals are aiming at the realization of cascaded FEL configurations, where a seed signal at the wavelength λ is used to modulate the beam density with periodicity λ and to generate radiation at λ/n in a radiator section tuned at the harmonic n. The procedure is repeated to generate radiation at $\lambda/n*m$ by seeding another modulator/radiator with up-conversion to the m-th harmonic [15][16][17]. This cascaded sequence can in principle be used to reduce the seed wavelength below the nm and reduce the requests in terms of beam energy and device costs (e.g. BATES (MIT, USA) [17]). It is playing a primary role in the design of FEL facilities like BESSY [9], ARC-EN-CIEL (Accelerator-Radiation Complex for ENhanced Coherent Intense Extended Light, France) [8], FERMI [11], MAX-4 [12] and SPARX [13], and it will affect the design of future FEL facilities.

1.2. Seed sources

Important progresses in the field of strong laser-matter interaction have been made, leading to the generation of high-order harmonics of intense laser pulses in gases. This technique is being well controlled. It is possible to obtain radiation with high energy per pulse down to 10 nm [18]. It has been proposed to use these High-order Harmonics of a laser, generated in a Gas (HHG), as a seed to feed a high-gain FEL amplifier, which radiates at $\lambda/3$ or $\lambda/5$, and to extract the Non-linear Harmonics Generated (NHG) [19]. Seeding with harmonics generated in gas has been experimentally proven in X-ray laser plasma pumped by OFI (Optical Field Ionization) in a gas jet [20]. The harmonics produced in gas seem to be a very good candidate to seed an FEL cascade, to extend the operating wavelength range of FELs to the "water window" (2.33-4.37 nm) and probably down to sub-nm wavelengths. The harmonic multiplication process is however affected by the amplification of the intrinsic noise existing in the seed and that induced by the e-beam natural shot noise. In ref. [21] it has been pointed out that the signal to noise (S/N) ratio is affected by the amplification of any phase/amplitude distortion from one FEL stage to the next. This result would make impossible the realization of multistage cascaded FELs with large harmonic multiplication factors. Fortunately another mechanism, which is associated with the natural FEL radiation slippage over the electron pulse, limits the FEL gain bandwidth and allows to keep under control the noise growth. In ref. [16] a multiplication factor of 240 has been demonstrated in a fully 3D time dependent numerical simulation by properly tuning the configuration parameters. Non-linear effects associated to the combined processes of saturation and slippage may also be exploited in order to suppress the growth of noise and to increase the cascaded FEL stability with respect to external perturbations [22]. The possibility of testing these schemes, as well as a better understanding of the noise propagation effects through a cascade and the associated problems, will affect the design of all FEL facilities foreseen in the future and may also influence the near future development of ongoing ones.

1.3. Seeding @ SPARC

The experiment on SPARC [23] *(Sorgente Pulsata e Amplificata di Radiazione Coerente, Italy)* consists in installing a secondary laser amplifier chain which is devoted to the amplification and conversion to higher order harmonics of a short laser pulse, equivalent to that coming from the oscillator which drives the photocathode. This pulse is then injected into the SPARC undulator as a seed for the FEL amplification process. The high-order harmonics can be generated in crystal, at the wavelength of 400 nm and 266 nm, or in gas jet (or in a gas cell), according to the process described in Sec. 3.2. Diagnostics of the output radiation in terms of spectrum and pulse duration provide relevant information about the FEL amplification process. The SPARC configuration is monitored by diagnostic stations located in between the six undulator sections, which provide the opportunity to follow the dynamics of the pulse propagation in different FEL regimes, from the shot noise to the exponential growth, to the saturation and beyond. The radiation diagnostics on the harmonics of the fundamental allow to monitor the bunching process at higher frequencies along the undulator as well.

This experiment and the associated R&D have many outcomes and possibilities:

1 - Study of the problems related to the injection of an external radiation seed in a single pass FEL. Analysis of the coupling efficiency of the e-beam – seed pulse in terms of the input parameters.

2 - SPARC as a FEL/beam dynamics test facility offers the possibility of performing experiments of seeding, analysing both the spectral and time domain pulse properties along the undulator. The e-beam shot noise suppression induced by the coherent seed at different wavelengths can

be studied. A comparison with simulation data will allow code validation for extrapolation of the simulation data to lower wavelengths.

3 - The evolution of phase/amplitude perturbations of a smooth pulse can be analysed in different conditions of gain saturation and slippage. Strongly non-linear regime of FEL operation can be induced and experimentally verified.

4 - The implementation of a DAZZLER, a device that allows phase and amplitude filtering of the frequencies of a given input signal, installed after the synchronized oscillator allows the production of two short input seeds delayed by a fraction of the electron pulse length, and possibly shifted in frequency. The analysis of these pulses in the frequency domain, e.g., using the SPIDER technique [24], should allow to follow the phase of the amplified signal which can be compared to the phase of the input signal.

5 - The above analysis can be extended to the harmonics produced in SPARC. The seeding in the present SPARC configuration is possible at 266 nm (3rd harmonic) and at 160 nm (5th harmonic). Future developments may allow to seed down to 114 nm (7th harmonic) and 90 nm (9th harmonic). At the shortest wavelengths the FEL is operated exploiting the gain on higher order harmonics thus extending the SPARC operating range down to the EUV.

6 - The SPARC variable gap undulator can be operated at different resonant frequencies, thus allowing tests of cascaded FEL configurations.

7 - An experimental test of Super-radiance in a single pass FEL can be implemented, and the interesting properties of a Super-radiant pulse in a cascaded FEL can be experimentally studied.

8 - The flexibility of the SPARC variable gap undulator could be exploited to test the *fresh bunch injection technique* **Errore. L'origine riferimento non è stata trovata.**, which has been considered as a mean to overcome the e-beam heating which inhibits the gain process in a multiple stage FEL cascade.

The simultaneous availability of a FEL based on a state-of-the-art electron beam and a high power laser that can be exploited for seeding experiments opens a wide number of possibilities for experiments aimed at a deeper understanding of the FEL physics. These experiments are of paramount importance for opening new breakthroughs in the physics and technology of short wavelength FELs and have the potential to drive the design of new light sources as SPARX [13].

2. Description of the collaboration and participants

2.1. Introduction

The experiment is the result of a collaboration between several groups from different European Institutes. In the following a description of the various partners is given together with a brief summary of the partner's role in the collaboration.

2.2. Politecnico di Milano - National Laboratory for Ultrafast and Ultraintense Optical Science - ULTRAS

ULTRAS is a Research Centre of the "National Institute for Physics of Matter (INFM)" and it is located at the Department of Physics of Politecnico of Milan (Italy).

The aim of ULTRAS is to combine both aspects of extreme time resolution (few optical cycle pulses) and high peak power for a variety of applications in gas and solid state physics, plasma physics, surface science and photobiology. ULTRAS provides expertise in the development of ultrashort laser sources and related technologies, as well as in surface science and in photobiology. The main research activities carried out can be summarised as follows: (i) Generation of ultrashort X-UV radiation (by high order harmonics in the soft X ray region using few optical cycle pulses); (ii) Ultrafast spectroscopy from visible to near-IR (for investigating ultrafast relaxation processes in organics and optical properties of biological tissues); (iii) Femto-spectroscopy in the XUV (for investigating core level transitions of metals and the rare earths, and for valence band photoemission experiments with fs time resolution); (iv) Attosecond technology and physics (development of lasers and optical technology towards generation and application of attosecond pulses). Exploratory research lines in emerging fields are, namely: Nano- and micro-machining of active and passive materials (waveguide fabrication with innovative lasers and focusing schemes), and Femtosecond nano-optics (new concepts in aperture-less and time-resolved aperture near-field scanning optical microscopy).

ULTRAS is the major bodies of the facility "Centre for Ultrafast Science and Biomedical Optics" (CUSBO), which has been recognised by European Union eligible to the program of "Access to large scale infrastructures" both in the V and VI Framework Program. and therefore open to European users. ULTRAS counts over 24 researchers, an average of 14 PhD students and several post-Docs.

ULTRAS will bring into the collaboration for the S*eeding@SPARC* experiment its know how relevant to the optimization of the laser system for generating high order harmonics, studying new techniques for the measurement of time duration of very short pulses in the UV and VUV range of the spectrum.

2.3. Università di Padova (INFM – LUXOR)

LUXOR (Laboratory for Ultraviolet and X-ray Optical Research) is a research center of the "National Institute for Physics of Matter (INFM). LUXOR is located at the physics department of "Ingegneria dell'Informazione" of the University of Padova. This laboratory is involved in basic and applied research projects. Researchers both from the University and the INFM cooperate at the LUXOR activities mainly funded by the main Italian and European research institutions and private companies. The laboratory is experienced in the design and realization of optical systems for scientific applications (aerospace and matter physics applications) and industrial applications, in the test and characterization of optical devices and detectors, mainly focused to the vacuum ultraviolet wavelengths range, in the development of conventional and semi-conductor lasers for industrial applications, in the implementation of X-ray monitoring in industrial processes.

LUXOR will bring into the collaboration for the *Seeding@SPARC* experiment its know how relevant to the development of optics for radiation transport, monochromators and spectromenters for the measure of the wide band spectra generated by the seeded SPARC FEL. The development of a wide band spectrometer in the range 500 – 40 nm is one of the main tools of radiation diagnostics for SPARC both in SASE and seeded mode and the contribution of LUXOR is considered essential.

2.4. University of Rome I "La Sapienza"

The University of Rome I "La Sapienza" has been involved in the SPARC project from its beginning and has contributed to the development of various elements of the SPARC injector, collaborating in particular with the photocathode laser, the radiofrequency gun and with the diagnostic and controls groups. With experimental expertise in high-brightness electron beam, in the synchronization of different laser systems and in the interaction of relativistic electrons with high power laser beams, this group will constitute an important support to the *Seeding@SPARC* project. On the theoretical side, the University of Rome I "La Sapienza" group will contribute with fully 3D FEL simulations and models that will help in designing and predicting the outcome of the various proposed seeding scenarios, and at the same time, will constitute an important tool for advanced studies and research in the non linear FEL dynamics.

2.5. CEA

CEA-SPAM (Service de Photons, Atomes et Molécules) has expertise in FEL studies, operation of the Super-ACO free electron laser, dynamical studies and first user applications, pulse shaping (using DAZZLER and SPIDER), harmonic generation in gas in the VUV. It contributes to laser and synchronisation, seeding and harmonic generation. The Laboratoire des Solides Irradiés, Ecole polytechnique, Palaiseau, France, investigates the interaction of radiation with materials and the electronic structure of solids (theory). In the consortium it contributes to the photoinjection task. The fields of excellence of CEA-SACM (Service des Accélérateurs et du Cryomagnétisme) are: High energy and nuclear physics, research, development, construction and operation of particle accelerators (beam dynamics, superconducting RF technologies, high magnetic field technologies), computing, remote operation systems.

The group from CEA will design and build the chamber for the generation in gas jet of high order harmonics of the Ti.Sa laser (HHG). The partecipartion will bring into the collaboration the experience this partner in the HHG process, in the sub-ps laser pulses manipulation and in the radiation diagnostics that will be implemented in collaboration with the ULTRAS group from Politecnico fo Milan.

2.6. INFN

The INFN - the National Institute of Nuclear Physics - is an organization dedicated to the study of the fundamental constituents of matter, and conducts theoretical and experimental research in the fields of subnuclear, nuclear, and astro-particle physics. INFN is currently building an advanced photo-injector system at the Frascati INFN National Laboratories (LNF) to conduct a SASE-FEL test experiment (SPARC project) in the context of a wider activity for the design of a soft X-ray SASE-FEL Italian facility.

Specific roles in the consortium: drive laser system and cathodes developments, design, construction and test of a longitudinal beam compression with RF techniques, gun diagnostic simulations and construction; beam dynamics simulations and verification of codes, controls and synchronization development; simulation and design of SCRF guns.

INFN is hosting the SPARC experiment at the LNF institute. The institute will provide the compulsory support for the experiment setup from the logistic and technical point of view. A close scientific collaboration covering the laser system set-up, synchronization of the laser/electrons beam, and the SPARC-Linac driver is essential for the success of the *Seeding@SPARC* experiment.

2.7. ENEA

Pioneer in FEL theoretical and experimental activity with long dated expertise in the fields of microwave engineering, accelerators, undulators, optical design and diagnostics. At ENEA was realized the first FEL operating in the infrared region of the spectrum based on a microtron as electron souce and is presently operation a FEL THz facility. ENEA is partner in several European projects related to the study, development and applications of FELs, and leading contractor of the Italian SPARC project. ENEA will contribute to the *Seeding@SPARC* experiment with novel studies in FEL related beam dynamics, synchronization issues, seeding and harmonic generation. ENEA is coordinating the *Seeding@SPARC* working group that is defining the details of the experiment.

3. Conceptual Experiment Description

3.1. Introduction

The experiment consists in operating the SPARC FEL amplifier with an external input seed and analyse the optical pulse evolution along the undulator. The seed is generated by non-linear up conversion of a Ti:Sa laser signal, in a crystal at the wavelengths of 400 nm and 266 nm and in a gas jet, at the wavelengths of 266 nm, 160 nm. Depending on the conversion efficiency achieved in the gas jet, the wavelengths of 114 nm, 88 nm and lower can be also explored. The mechanism of harmonic generation in gas is briefly described in Sec.3.2. The implementation of the harmonic generation system at SPARC is analyzed in detail in Chapter 5. The FEL amplification at the shortest wavelengths (below 114 nm) cannot be reached by increasing the e-beam energy, which is limited to the maximum design value of 200 MeV, but may be reached by operating the SPARC undulator on a sub-harmonic of the seed and exploiting the gain process on higher order harmonics. A brief analysis of the undulator/beam parameter space and the wavelength of operation of the seeded SPARC configuration is shown in Sec. 3.3.

The first expected effect of the presence of a seed is that of shortening the saturation length of the FEL, as it was pointed out in ref.[26]. When operated in SASE mode with the working point parameters specified in ref.[27], the SPARC FEL cannot reach saturation in the UV on the fundamental harmonic. In the detailed analysis of Sec. 3.5 it is shown that SPARC in seeded mode, operating with an electron beam with the parameters shown in Sec. 3.4 may reach saturation on the fundamental harmonic down to 114 nm if a suitable seed is generated.

A wavelength range extension of the SPARC source is only one of the benefits of seeding. Other expected effects consist in a reduction of the shot to shot fluctuations with respect to the SASE operation that should be accompanied by a consistent bandwidth narrowing that should bring the optical pulse close to the Fourier limit. Some of the possible experiments which have been listed in Sec. 1.3 are

- Harmonic generation in a FEL can be studied by measuring the harmonic conversion efficiency by seeding the FEL with an intense seed close to FEL saturation.
- The distributed diagnostics of the SPARC FEL allow to follow the evolution of the FEL signal along the undulator. A suitable seed can be then used to test experimentally the solitary wave-like behaviour of superradiant pulses [28].
- The flexibility of the SPARC undulator also allows to test cascaded FEL configurations, by setting the undulators at different gaps.

The implementation of seeding at SPARC requires some modifications to the present SPARC layout. The following main items are required:

- A new laser hutch should installed closely to the present laser clean room where the laser pulse required for the photoemission at the cathode is generated. This laser room should host the secondary laser amplification line where the pulse for harmonic up-conversion in crystal or in gas is prepared.
- The chamber for the harmonic conversion in gas must be installed at a short distance from the e-beam line, in order to minimize the number of optical elements required to match the seed light to the e-beam itself.

- A small chicane must be installed along the beam path in the transfer line to allow the injection of radiation in the first undulator, which is superimposed to the electron beam both in the transverse and in the longitudinal plane.

A layout of the SPARC room with the seeding LASER room, the IR transfer line and the two chambers for the generation of harmonics in gas is shown in Fig. 1.

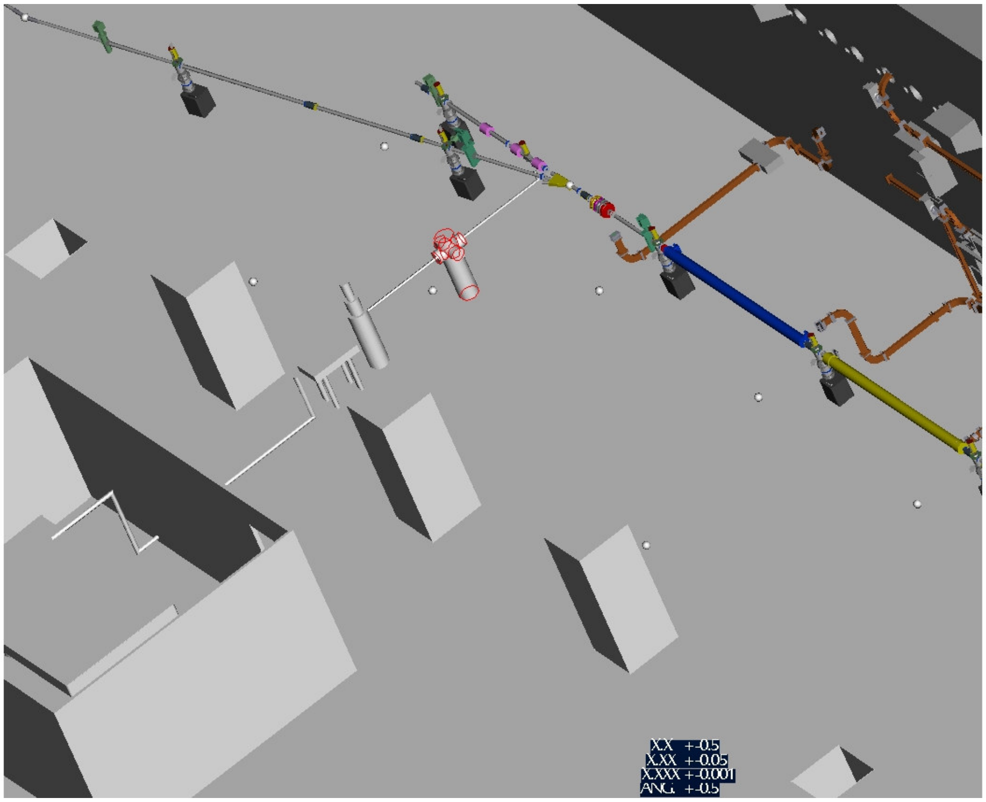

Fig. 1. *Three dimensional view of the SPARC room with the laser hutch for the seeding laser, the IR transfer line and the chambers for harmonic generation in gas*

The temporal superposition is obtained by phase locking the seed laser with the laser driving the photocathode and a remotely controlled delay line (See Sec.7.3 for details). The spatial superposition is obtained by inserting a mirror along the electron path before the undulator. In Fig. 2 it is shown a detailed view of the SPARC transfer line between the Linac and the undulator sections.

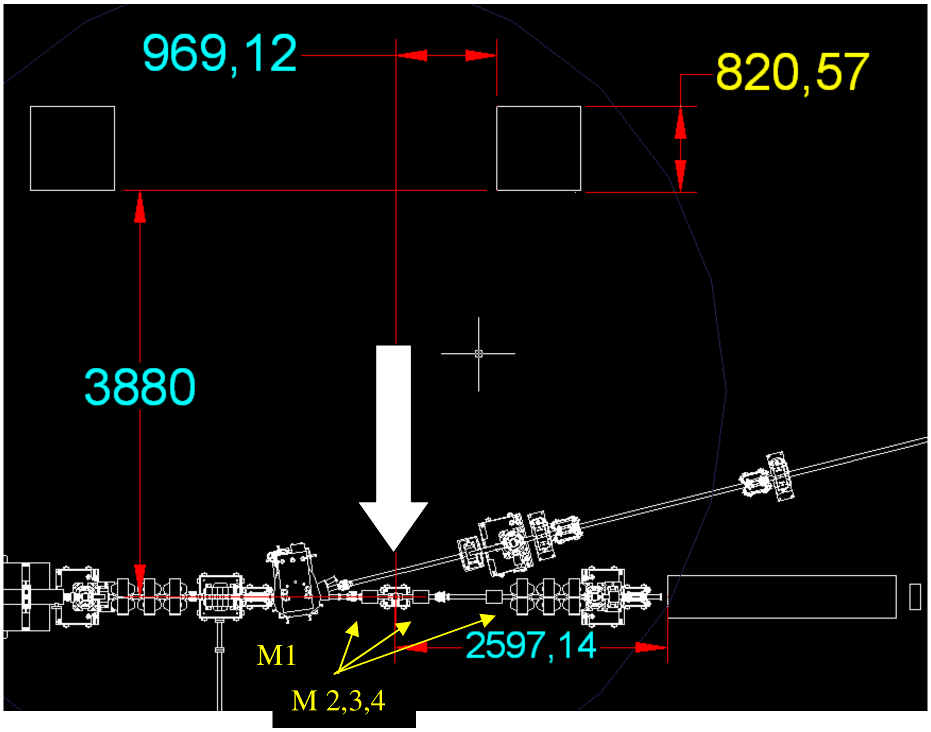

Fig. 2. *Detail of the SPARC layout representing the transfer line between the SPARC Linac and the Undulators. The white arrow indicates the diagnostic chamber where a mirror at 45° can be located to inject the seed inline in the undulator.*

A suitable position where this mirror can be located with a minimal interference with the SPARC-Linac diagnostics is the diagnostic chamber indicated with a white arrow in Fig. 2. A mirror at 45° is the last element of the seeding optical beamline. In order to avoid interaction between the e-beam and the mirror the e-beam is deflected from the straight orbit by means of a small chicane realized with the large bending magnet M1 (see Fig. 2) and by three small magnets correcting the orbit before the last triplet ($M_{2,3,4}$ in Fig. 2). An orbit displacement between 5 and 10 mm is sufficient to accommodate a small mirror of 6 mm of diameter into the chamber. This displacement can be realized within the existing vacuum chamber which has an inner diameter of 40mm. The normal straight orbit of the SPARC beam may be recovered by switching off the magnets and by moving the mirror on one side of the chamber. A detailed analysis of the problems connected with the modifications required in the transfer line is shown in Sec. 4.

3.2. Harmonic generation in GAS

One of the distinguishing features of this experiment is the nature of the radiation source used for seeding. The harmonic generation in gas is indeed one of the most promising methods to generate radiation at short wavelengths, in the VUV – EUV region of the spectrum, which can be used as and input seed for a short wavelength Free Electron Laser. The high order harmonics result from the strong non-linear polarisation induced on the rare gases atoms, such as *Ar, Xe, Ne* and *He*, by the focused intense electromagnetic field E_{Laser} of a "pump" laser. The most important characteristics of the process are given by the three-step semi-classical model [30][31] illustrated in Fig. 3. As the external electromagnetic field strength is comparable to the internal static field V_c of the atom in the interaction region close to laser focus, atoms ionize by tunnelling of the electrons. The ejected free electrons, far from the core, are then accelerated in the external laser field and gain a kinetic energy E_C. Those which are driven back close to the core can either be scattered or recombine to the ground state emitting a burst of XUV photons every half-optical cycle

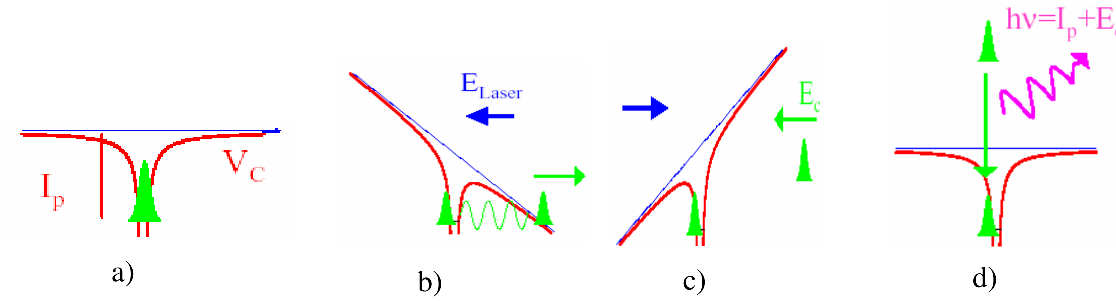

Fig. 3. *Three-step semi-classical model a) initial state of the gas atom at zero field, V_C : Coulomb potential, I_p : ionization potential b) electron tunnelling c) electron acceleration and gain of kinetic energy E_C d) radiative recombination and emission of XUV burst*

Correspondingly in the spectral domain, the harmonic spectrum (see Fig. 4) includes the odd harmonics of the fundamental laser frequency. The characteristic distribution of intensities is almost constant with harmonic order in the "plateau" region where, depending on the generating gas, the conversion efficiency varies in the range 10^{-4}-10^{-7}. For higher orders, the conversion efficiency decreases rapidly in the "cut-off" region.

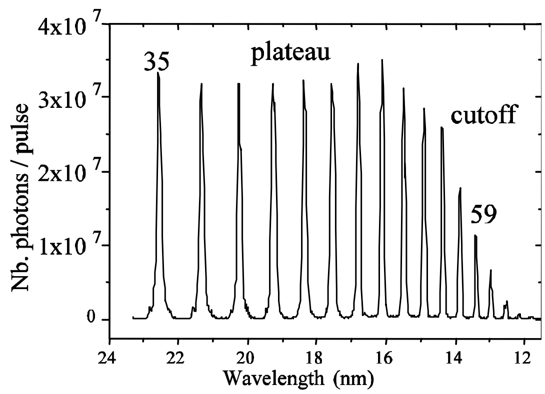

.

Fig. 4. *High Order Harmonics spectrum in Ne.*

The upper spectral limit is given by the so-called “cut-off law”, $E_{cutoff} = V_P + 3.2\ U_P$, where V_P is the gas ionization potential, $U_P \propto I_{pump}\ \lambda^2_{pump}$ is the ponderomotive potential (I_{pump} the focused intensity, λ_{pump} the wavelength of the pump). According to the three-step model and the cut-off law, the lighter the gas, i.e., the higher the ionization potential and the laser intensity which can be applied without ionizing the atom, the higher the cut-off energy.

Moreover, the radiation spectrum is completely tuneable in the VUV-XUV region by means of frequency-mixing techniques applied on the pump laser [32]. High order harmonics are linearly polarized sources [33] between 100 and 3 nm (12-400 eV), of high temporal [34] and spatial [35] coherence, emitting very short pulses (less than 100 fs), with a relatively high repetition rate (up to few kHz). The harmonic radiation is emitted on the axis of the laser propagation with a small divergence (1 to 10 mrad).

In Fig. 5 it is shown a plot with the state of the art of the sources of high order harmonics generated in gas with a pulse length of 50 fs from various noble gases. A considerable amount of radiation is emitted down to 10 nm with the *Ne* gas.

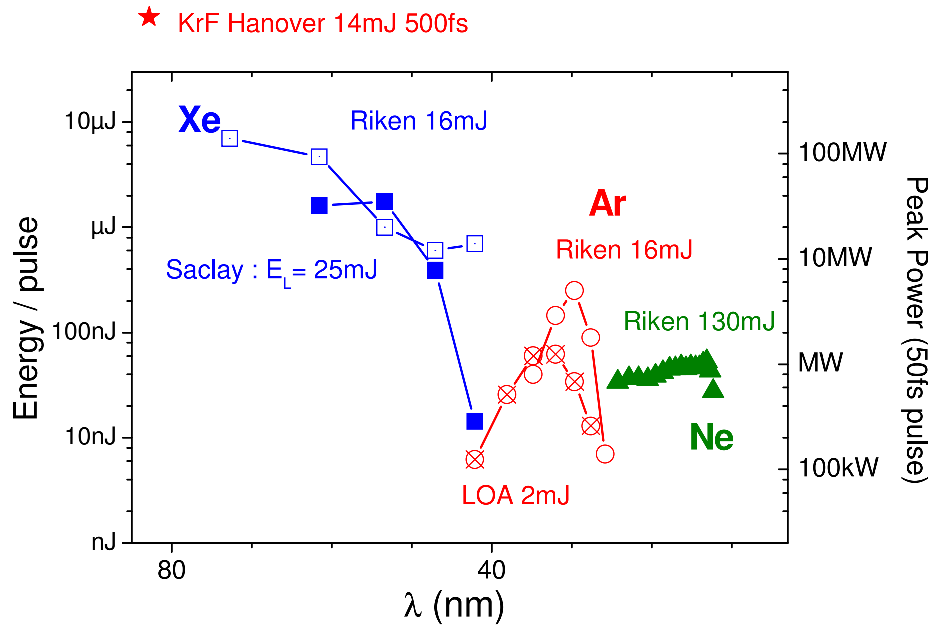

Fig. 5. *Energy per pulse obtained with the high harmonic generation in gas technique. The references considered in drawing the above plot are: Riken[36][37][38][39], Saclay [40], LOA [41], Hanover[42]*

In the specific case of SPARC the emission is required at the harmonics up to the ninth (88 nm) and the energy per pulse may be relaxed with respect to the 160 mJ required to reproduce the results published at *Riken.* In Sec.5 a detailed analysis of the implementation of the harmonic generation system is given.

3.3. The SPARC undulator

A description of the SPARC undulator may be found in ref.[43] The undulator is composed by 6 sections of 75 periods each. The main undulator parameters are summarized in Tab. II.

Tab. II. *Main undulator parameters*

Period	2.8 cm
No of Periods	77 (effective number is 75)
Gap (nom./min/max)	0.958 / 0.6 / 2.5 cm
K (nom./max/min)	2.145 / 3.2 / 0.38

Assuming that the e-beam energy may be varied in the range 150-200 MeV, we have shown in Fig. 6 the dependence of the wavelength with the undulator *K* parameter in the gap range allowed by the undulator in the SPARC configuration. The second harmonic of the Ti:Sa may be reached at a beam energy of 170 MeV. At 200 MeV the odd harmonics of the Ti:Sa (266 – 160 and 114 nm) may be reached by varying the undulator gap.

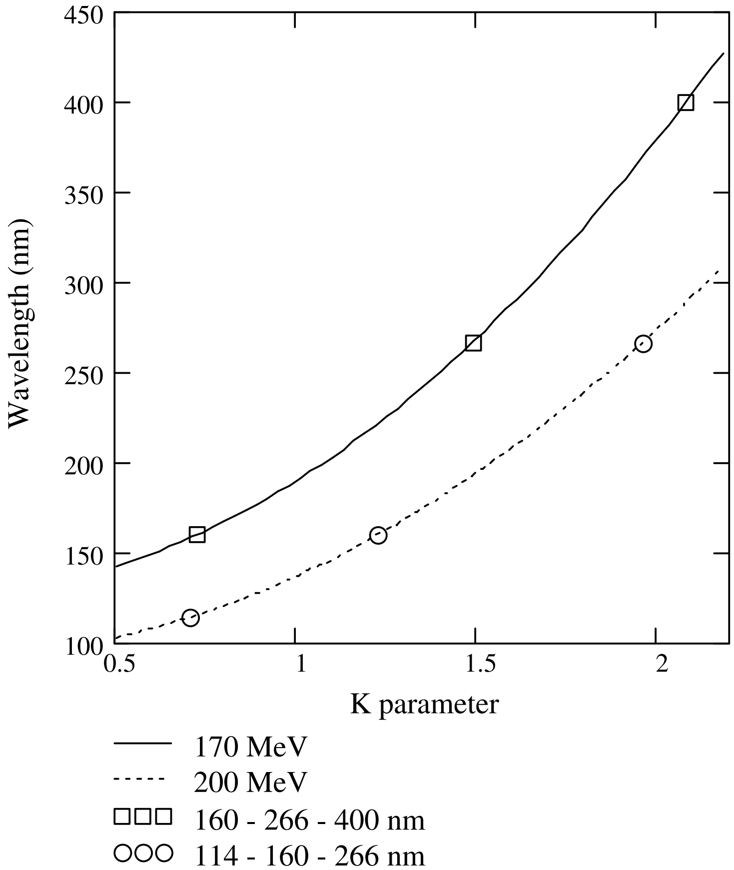

Fig. 6. *Resonant condition at the e-beam energy of 170 and 200 MeV. The symbols show the values of the K parameters required to set the resonance at the harmonics of the Ti:Sa laser.*

The wavelength of 88 nm may be reached by tuning the undulator at the gap corresponding to the resonance at 266 nm and by seeding at the third harmonic. This configuration is particularly interesting to measure the gain at the third harmonic as a method to extend the operating range of an undulator.

3.4. Electron beam parameters at the undulator

The SPARC accelerator is composed by a 1.6 cell RF gun operated at S-band (2.856 GHz,of the BNL/UCLA/SLAC type) with incorporated metallic photocathode, generating a 5.6 MeV beam which is properly focused and matched into 3 accelerating sections of the SLAC type (S-band,travelling wave),which accelerate the beam to 155-200 MeV.

The detailed study of beam dynamics and the process of optimization of the working point including the study of tolerances in the SPARC injector has been done by using HOMDYN , PARMELA and TREDI codes and the results are reported and largely described in ref.[27].

We summarize here the main beam parameters and the foreseen characteristics of the beam at the entrance of the undulator that are relevant for the seeding experiment, as listed in Tab. III.

Tab. III. *SPARC beam parameters*

Energy (MeV)	155-200 MeV

Bunch charge (nC)	1.1
Repetition rate (Hz)	1-10
Pulse duration (flat top) (psec)	10
Pulse rise time 10%-90% (psec)	1
Bunch Current (A)	100
RMS normalized transverse emittance (mm-mrad)	<2
RMS normalized transverse slice emittance (mm-mrad)	<1
RMS long. Emittance (deg-KeV)	1000
RMS energy spread (total) (%)	<0.2
RMS energy spread (slice) (%)	<0.1
RMS bunch length (mm)	1

In Fig. 7 the behaviour of the normalized rms emittance and rms envelope in the X and Y planes are shown as computed by PARMELA with the space charge included. The values of the emittance compensation magnetic field placed near the gun, the gun phase, the cathode spot size and the position of the accelerating sections have been optimized in order to minimize the final normalized transverse emittance (0.7 mm mrad) for a beam current of 100 A.

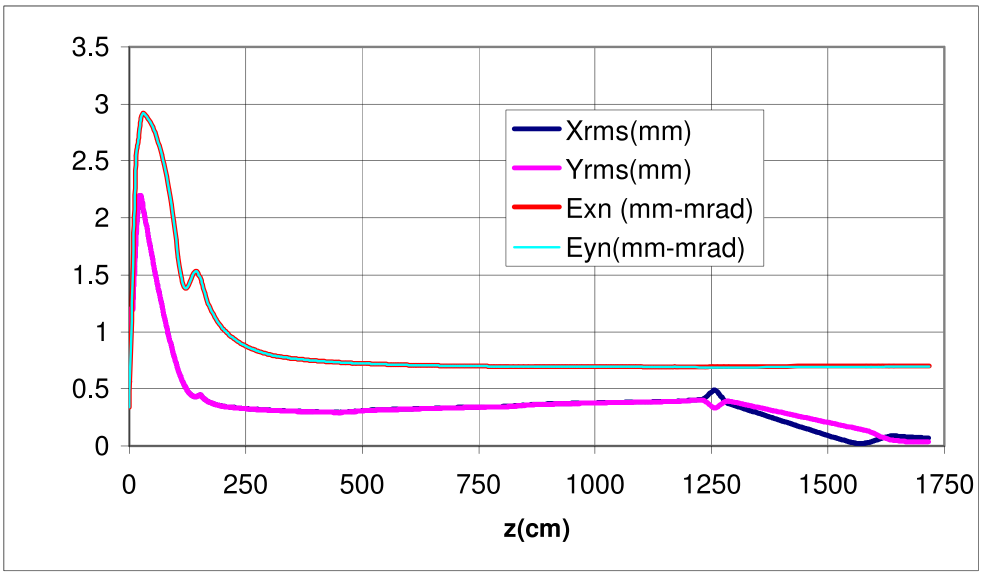

Fig. 7. *x and y rms normalized emittances and envelopes in the SPARC beamline from the gun to the undulator entrance*

The beam phase space at the end of the transfer line with space charge on and off is shown in Fig. 8. When the space charge is off the agreement between the ideal values and the values given by the tracking is within 15%, while the mismatching increases when the space charge effect is taken into account: in particular the mismatching occurs for the values of the Twiss parameters α_x and α_y as it is reported in . If we introduce a mismatching parameter [29] defined as

$$\xi = \frac{1}{2} \cdot (\beta_0 \gamma - 2\alpha_0 \alpha + \gamma_0 \beta) \qquad (1)$$

where the label *0* corresponds to the perfectly matched parameters, we have that the values of the Twiss parameters retrieved from the tracking give ξx=1.0026 and ξy=1.0032 with the space charge off and ξx=1.02 and ξy=1.03 with the space charge on. FEL calculations show that these values are well within the FEL tolerances.

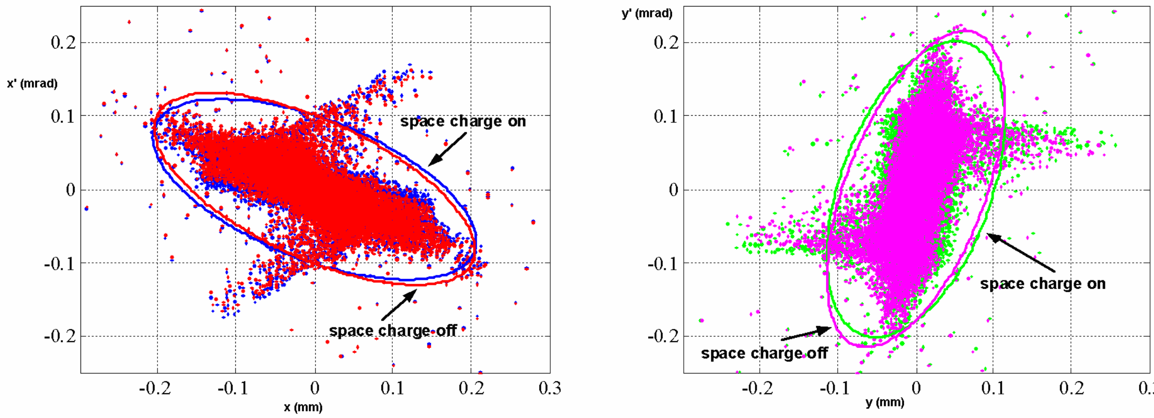

Fig. 8. *PARMELA computed X-X' and Y-Y' phase space at the end of the transfer line with the space charge on and off in the transfer line.*

Tab. IV. *PARMELA computed Twiss parameters at the undulator entrance in the nominal configuration*

Twiss parameters at the end of the transfer line*	Required values	PARMELA values with space charge off in the transfer line	PARMELA computed values with space charge on in the transfer line
αx	0.878	0.82	0.697
βx (m/rad)	2.00	2.03	2.04
αy	-0.787	-0.69	-0.505
βy (m/rad)	0.68	0.64	0.637

As to the slice analysis it gives for a slice length of 300 μm in the range of operation energies of SPARC the results shown in Fig. 9: in the central part of the beam the slice normalized transverse emittance is not larger than 0.6 mm-mrad, the maximum slice current is ~ 110 A, the slice energy spread is ≤0.6 % and a percentage of 66% of the beam has a current ≥ 100A.

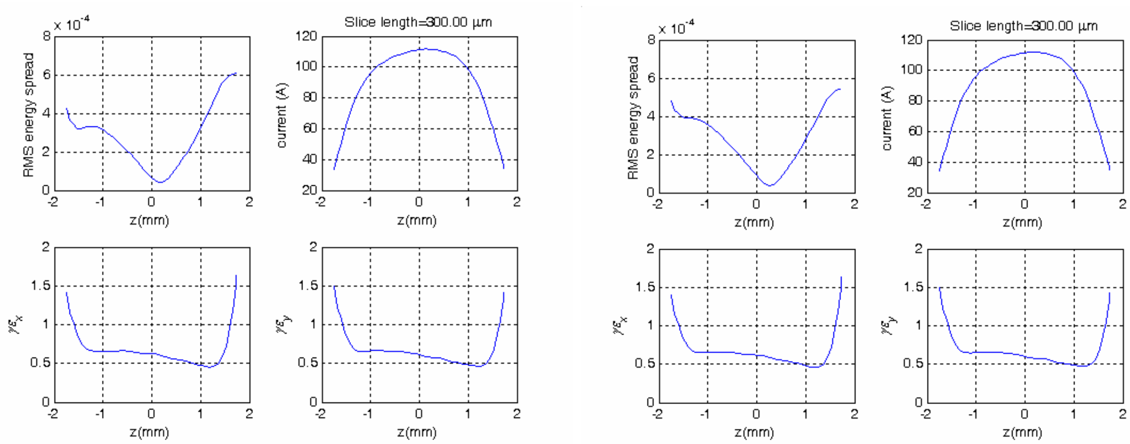

Fig. 9. *Slice analysis of SPARC beam at the entrance of the undulator: (a) energy=155 MeV (b) energy=200 MeV.*

3.5. Optical injection scheme and seeded FEL simulations

In order to preserve flexibility and allow experiments with the higher harmonics of the Ti:Sa laser generated both in a non linear crystal and in a gas jet, we considered different cases of radiation wavelengths: 400 nm, 266 nm, 160 nm, 114 nm.

Few different optical schemes were considered for the injection of the short wavelength radiation seed collinearly with the electron beam. Because of the existing hardware constraints and the fact that the seed radiation and the e-beam have very similar emittances, we chose to deviate the e-beam from its rectilinear path. In fact we considered both the solution of a mirror with a hole, and of a collinear higher harmonic gas generation. The latter was excluded by the constraints of space available in the SPARC beam-line, while the former was impossible to realize because the sizes of the laser and electron beam turned out to be comparable at the location of the insertion mirror.

We show in Fig. 10 the scheme considered here. A four bending magnet chicane has been designed to deviate the e-beam off axis by an offset of few mm, and to create the room necessary to insert a mirror to reflect the radiation on the undulator axis (Details are given in SEZIONE). The radiation pulse of power P and wavelength λ co-propagates with the electron beam after the last mirror reflection, focuses at a distance z_w from the undulator entrance to a spot size *w*, and is characterized by a Rayleigh range z_r.

Firstly, we tried to optimize the energy/information exchange between the radiation and the particles varying the Rayleigh range and the location of the laser waist inside the undulator. One wants to maximize the seeding radiation intensity in such a way that the bunching is written on the electron beam as early and as efficiently as possible. In other words, we look for the configuration of z_r and z_w that with the same input power reaches the exponential gain regime earlier in the undulator. This analysis is reported here for the case of λ_{seed}=266 nm. This case is easily extendable to the other wavelengths.

The analysis is performed with the three dimensional FEL simulation code GENESIS 1.3. This code assumes a TEM00 Gaussian mode as a seed and then solves for the motion of the electrons and the evolution of the field in the undulator. It can also be run in the time-dependent mode to include the effects of the slippage and of the amplification of the spontaneous emission.

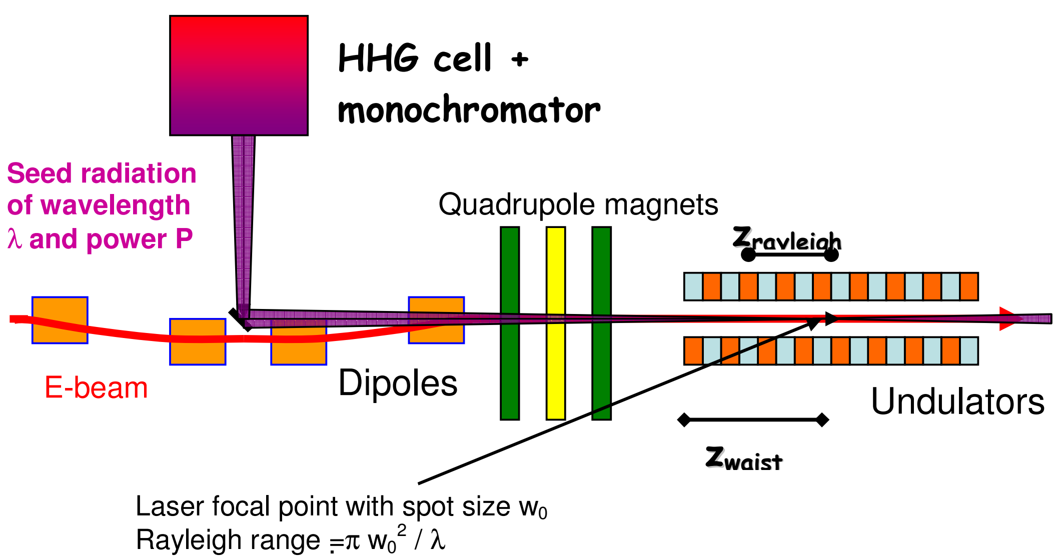

Fig. 10. *Seed radiation injection scheme*

The first thing that appears from the simulations is that a change in the diffraction pattern of the radiation implies a small change in the longitudinal k_z so that the resonant wavelength slightly shifts inside the larger FEL gain bandwidth. Because of this effect, for every simulation (i.e. each different z_r and z_w) case we first had to find the wavelength of the maximum gain and then compare the evolution of the bunching and the radiated power. The variation of the optimum wavelength case is easily calculated by writing down the variation of k_z changing z_r and z_w:

$$\Delta\lambda(z) = \frac{\lambda_0 \lambda_u}{2\pi z_{rayl}} \cdot \frac{1}{1+\left(\frac{z - z_{waist}}{z_{rayl}}\right)^2} \tag{2}$$

To find out the effect of this wavelength shift, one can average this expression over the first few gain lengths where the wavelength/phase information is written on the electron beam. In Table 3.3.1, we report the results of the simulations, explicitly indicating the resonant wavelength and the wavelength shift, due to the diffraction of the seed radiation.

As it appears from the other columns of Tab. V, it turned out that for a large range of possible seeding optical schemes the variation of the FEL performances are relatively small and can be easily compensated by a small increase in the seed power. In other words, the z_r and z_w parameter choice is not a critical one, since only a variation of 10% in the performances of the FEL amplifier (namely the distance over which the bunching parameter *B* reaches the 0.2 value) is found as we vary z_r and z_w.

We also calculated the projected spot size of the radiation at the injecting mirror location for all of the case studied. Since the size of the mirror is about 6mm and the *1/e2* amplitude of the radiation is in all case considered much less than the radius of the mirror, the diffraction losses are less than 0.1 % of the intensity. The mirror is a disk of 6mm

Tab. V. *Results of optimization of optical scheme for injecting the seeding radiation.*

z_r(m)	z_w(m)	λ_{res} (nm)	$\Delta\lambda$(nm)	Integrated K_l (10^{-6})	*B*=0.2 length (m)	Spot on injection mirror (mm)
0.5	1	267.1	1.31	3.7	3.72	1.46
0.5	0.5	266.9	1.21	3.6	3.68	1.25
0.2	1	266.9	1.1	3.2	4.1	2.28
0.7	0.7	266.9	1.1	3.75	3.66	1.14
4	1	266.4	0.3	1.6	4.3	0.77
0.2	0.2	267.1	1.33	3.3	3.95	1.77
2	1	266.6	0.6	2.6	3.91	0.83
0.2	0	266.8	0.87	2.7	4	1.63
0.5	0	266.7	0.75	2.8	3.84	1.05

The reason why the optical scheme does not influence critically the performances of the FEL amplifier, is that as soon as the exponential gain regime kicks in, the radiation beam size does not follow the behaviour given by the seed. As it can be seen in Fig. 11, gain guiding of the electromagnetic power starts and the radiation size is defined by the e-beam size. Because of this, it is sufficient to maximize the intensity of the radiation in the first gain lengths to find the optimum point of the optical scheme. The fifth column of Tab. V represents the results of this integration. K_l is the normalized vector potential associated with the laser wave and is defined as

$$K_l = 0.85 \cdot 10^{-9} \cdot \lambda[\mu m] \cdot \sqrt{I\left[\frac{W}{cm^2}\right]} \tag{3}$$

The integrated intensity for the wide range of z_r and z_w simulated does not change appreciably and this is the reason for the small effect on the FEL amplifier characteristics.

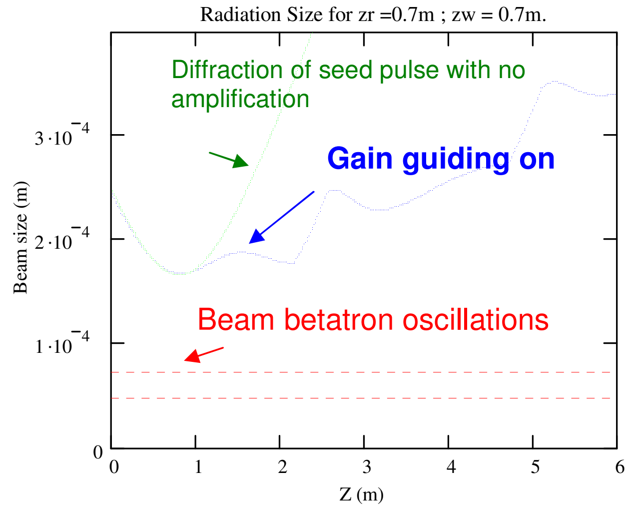

Fig. 11. *Radiation beam size along the interaction. The electron beam size oscillates between the red dotted lined. The laser beam size neglecting the gain guiding FEL effect is also shown in green.*

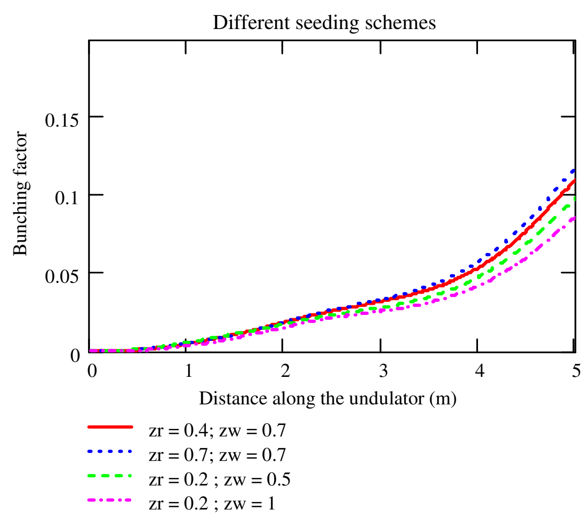

Fig. 12. *Evolution of the bunching parameters for three different seeding schemes*

The bunching factor at the resonant wavelength along the undulator is reported in Fig. 12 for few different cases of optical schemes. The differences between the optical schemes are less than 10% and can be easily compensated by an increase in the input seed power. These simulations are performed with an input seed power of 100 kW at a radiation wavelength of 266 nm.

The study of the different wavelength cases is summarized in Tab. VI. The maximum energy available from the SPARC linac is 200 MeV. In order to tune the SPARC undulators on the 5^{th} and 7^{th} harmonics of the Ti:Sa laser line, it is necessary to reduce the normalized magnetic field amplitude K by increasing the gap between the magnet poles, a possibility always available with the provided undulators. On the other hand, doing this reduces the coupling and it is the fundamental reason for the longer power gain lengths and higher input seed power needed to saturate.

Other options to go towards the short wavelength spectral region, avoiding an excessive decrease in the normalized K, include the possibility of seeding at an harmonic (for example the 3rd or the 5th) of the undulator resonant frequency.

The optical scheme can be maintained the same regardless of the radiation wavelength used, since the changes in the FEL amplifier performances are negligible. On the other hand, the last turning mirror should be chosen compatible with all the different wavelength seeding options.

A caveat must be made when looking at the saturation power numbers. The simulations here are done in the steady state regime, and do not include any slippage related effects. A summary of the simulation done at the different wavelength is shown in Tab. VI. In Tab. VII, Tab. VIII, Tab. IX and Tab. X are given the results for the second (400 nm), the third (266 nm) the 5th (160 nm) and the 7th (114 nm) harmonics respectively. The parameters in the tables represent the peak power, the rbs beam size and divergence, the pulse energy and the energy in the third harmonic in three positions along the undumlator: end of 1st undulator, end of 2nd undulator, and at saturation.

Tab. VI. *Summary of different wavelength simulations*

Resonant λ	**Beam Energy**	**Undulator K**	**Power Gain Length**	**Saturation Length with 100 KW input**	**Input Power to saturate**	**Power to overcome noise**
400 nm	175 MeV	2.17	0.51 m	6.5 m	~50 W	~50 W
266 nm	200 MeV	1.96	0.59 m	7.25 m	~200 W	~25 W
160 nm	200 MeV	1.22	0.96 m	12 m	7.5 kW	~15 W
114 nm[1]	200 MeV	0.7	1.3 m	>15 m	>100 kW	~5 W

Tab. VII. *Output radiation characteristics along the undulator for an input seed power of 100kW at 400 nm. The estimated energy radiated in the 5th harmonic (λ = 80 nm) at saturation is ~ 0.2 nJ.*

400 nm	**1st und**	**2nd und**	**Saturation**
Peak Power	1 MW	30 MW	55 MW
σ (rms)	250 μm	300 μm	400 μm
Divergence (rms)	0.4 mrad	0.4 mrad	0.3 mrad
E	100 nJ	3 μJ	5.5 μJ
E (3rd harmonic)	3 pJ	1 nJ	20 nJ

Tab. VIII. *Output radiation characteristics along the undulator for an input seed power of 100 kW at 266 nm. The estimated energy radiated in the 5th harmonic (λ = 53.2 nm) at saturation is ~ 0.1 nJ.*

266 nm	**1st und**	**2nd und**	**Saturation**
Peak Power	350 kW	10 MW	50 MW
σ (rms)	250 μm	300 μm	400 μm
Divergence (rms)	0.3 mrad	0.3 mrad	0.2 mrad
E	35 nJ	1 μJ	5 μJ
E (3rd harmonic)	1 pJ	0.5 nJ	10 nJ

[1] 114 nm simulation performed with 0.05 % energy spread.

Tab. IX. *Output radiation characteristics along the undulator for an input seed power of 100 kW at 160 nm. The estimated energy radiated in the 5^{th} harmonic (λ = 32 nm) at saturation is ~ 25 pJ.*

160 nm	1st und	2nd und	Saturation
Peak Power	200 kW	2 MW	25MW
σ (rms)	250 µm	300 µm	400 µm
Divergence (rms)	0.2 mrad	0.15 mrad	0.1 mrad
E	20 nJ	0.1 µJ	2.5 µJ
E (3rd harmonic)	<0.05 pJ	10 pJ	1 nJ

Tab. X. *Output radiation characteristics along the undulator for an input seed power of 100 kW at 114 nm. The estimated energy radiated in the 5th harmonic (λ = 32 nm) at saturation is ~ 0.5 pJ.*

114 nm	1st und	2nd und	Saturation
Peak Power	100 kW	0.4 MW	15MW
σ (rms)	250 µm	300 µm	400 µm
Divergence (rms)	0.15 mrad	0.12 mrad	0.06 mrad
E	10 nJ	40 nJ	1.5 µJ
E (3rd harmonic)	< 0.05 pJ	< 0.05 pJ	10 pJ

As a last consideration we have analysed the sensitivity of the FEL process to the input beam energy. In a SASE FEL the resonant frequency is determined by the gain spectrum which depends on the input beam energy. A jitter in the input energy induces an equivalent jitter in the central radiation wavelength. In a seeded FEL a jitter in energy still induces a jitter in the gain spectrum but the central frequency is determined by the seed and the result is a fluctuation of the gain, which means a fluctuation in the saturation length and of the output intensity. This effect has been analysed for the case with central resonant frequency at 266 nm. The simulations have been done with GENESIS in time dependent mode assuming a Fourier limited Gaussian seed pulse. This allowed to include the spectral broadening of the input seed associated to the pulse length (100 fs fwhm in this example).

Tab. XI. *Seeded FEL sensitivity (266 nm) to input beam energy jitter.*

Beam energy (MeV)	FEL output power (GW)	Pulse length (fs)	Saturation Length (m)
200.2	80	9.1	8.9
200.1	160	7.6	7.4
200	150	7.1	5.7
199.9	120	7.7	6.7
199.8	86	8.6	8.7

The parameters in Tab. XI are plotted in Fig. 13, Fig. 14 and Fig. 15 vs the input beam energy in a range of ±0.2%.

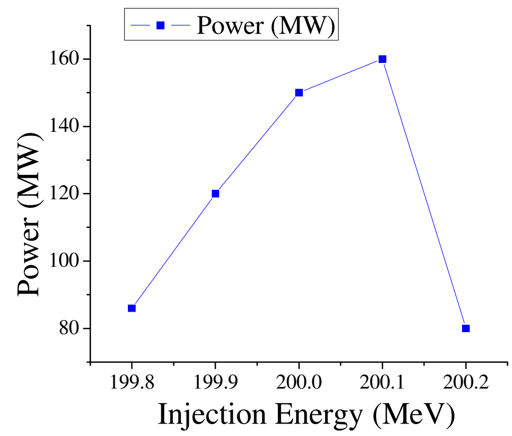

Fig. 13. *Output power vs. e-beam energy*

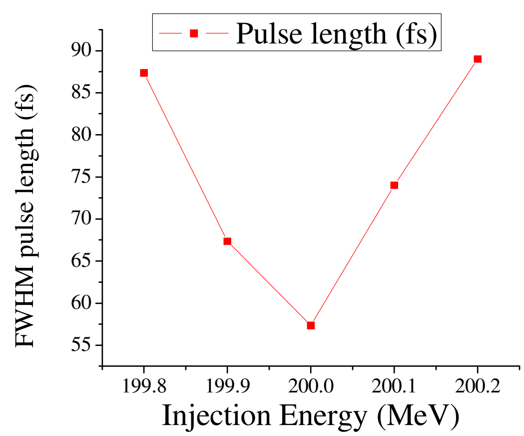

Fig. 14. *Laser pulse length vs. e-beam energy*

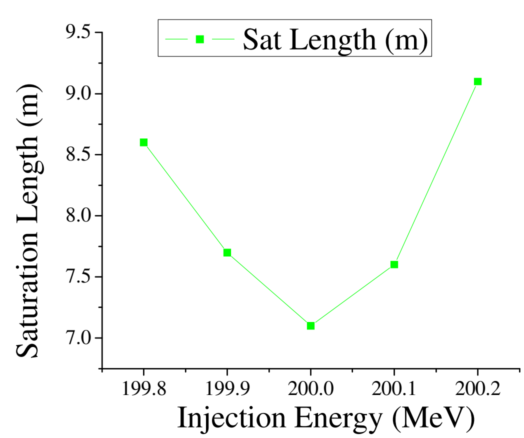

Fig. 15. *Saturation length vs. e-beam energy*

3.6. Harmonic generation in the seeded SPARC undulator

The FEL may be operated as a non-linear medium where high order harmonics can be generated. The gain process is not essential in this configuration. An intense input seed is injected in a single SPARC undulator section where the e-beam is modulated in energy and in phase according to the dynamics driven by the FEL-pendulum and the high order Fourier coefficients of the longitudinal current density appearing at saturation are responsible of a strong enhancement of the high order harmonics emitted in a linear undulator. This process can be investigated with a single undulator installed on the SPARC beamline and simulations of this simple configuration are in progress.

4. The injection system

4.1. Magnetic chicane layout

The transfer line from the SPARC linac exit to the undulator entrance, sketched in Fig. 16, is described in [2]. In the present configuration it is a 5.75 m long line including two triplets of quadrupoles, used for matching the beam parameters at the exit of the linac to those of the undulator beamline. The line includes also an RF-deflector placed at the exit of the first triplet for the measure of bunch length and slice beam parameters. The RF-deflector is followed by a bending magnet that will be used to deviate the beam towards the dogleg line (upper line in Fig. 16) used for beam compression studies.

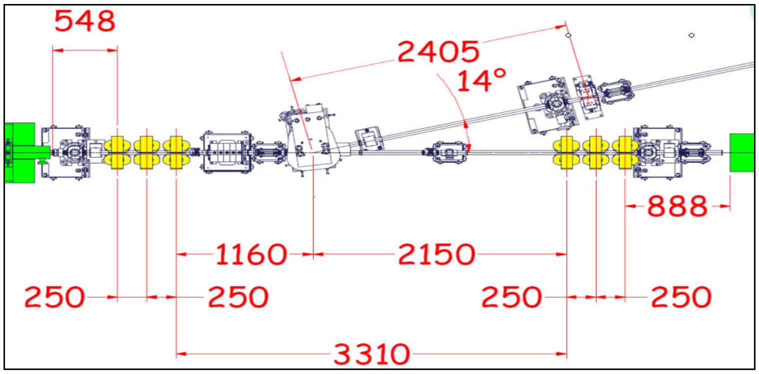

Fig. 16. *SPARC transfer line*

The layout of the transfer line has been modified in order allow the electron beam to perform a small "orbit chicane" and avoid interaction with the photon beam injected at the periscope, while they need to be superimposed at the undulator entrance. The required orbit bump is from 5 to 10 mm at the periscope location. The best solution is a four correctors scheme, which allows for having beam displacement and no angle at the desired injection location. Since the design of the transfer line has been already optimized for the SPARC working points at *155* and *200 MeV* electron energies, the best solution was to use as first bump corrector the first dipole of the dogleg. This solution allows to save space and to reduce at the same time the required corrector strengths. The flag and bellows positions, originally placed at the midpoint between the dipole and the second quadrupole triplet, had to be changed in order to accommodate the other *3* correctors. For the chosen corrector positions the required bump can be obtained with angles respectively of *7* and *14 mrad*. A layout of the modified transfer line is shown in Fig. 17.

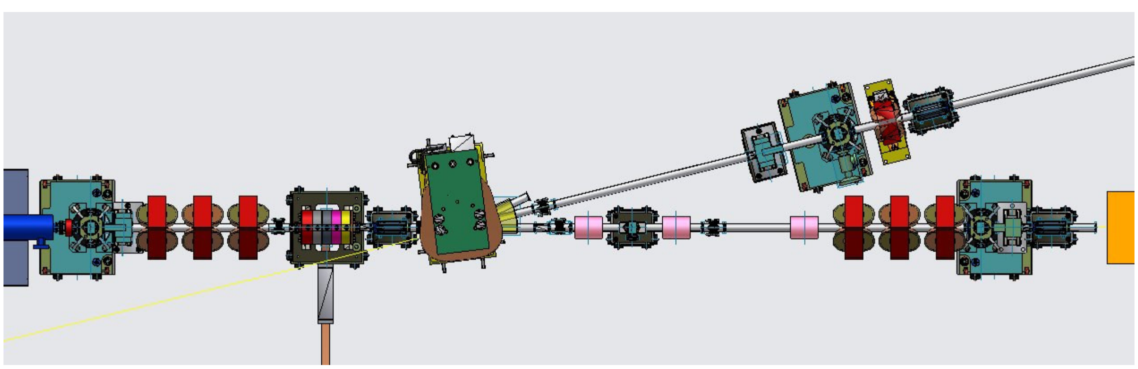

Fig. 17. *Top view of the transfer line layout, with the dipole in green and the three new correctors in pink. The periscope is between the first 2 new correctors.*

In the next section the required three new correctors are described in detail. The corrector locations and the required strengths are reported in Tab. XII.

Tab. XII. *Transfer line parameters*

Name	*L (m)*	*L_{tot} (m)*	*Θ (mrad) x 5mm*	*Θ (mrad) x 10mm*	*$K^2(m^{-2})$@ 155MeV*	*$K^2(m^{-2})$ @200 MeV*
Drift	0.498	0.498	-	-	-	-
Q1	0.10	0.598	-	-	-11.04	-10.62
Drift	0.15	0.748	-	-	-	-
Q2	0.10	0.848	-	-	+13.96	+13.78
Drift	0.15	0.998	-	-	-	-
Q3	0.10	1.098	-	-	-1.98	-2.13
Drift	0.98	2.078	-	-	-	-
Dipole	0.26	2.338	7.1429	14.2857	-	-
Drift	0.495	2.833	-	-	-	-
CX2	0.15	2.983	- 7.1429	- 14.2857	-	-
Drift	0.09	3.073	-	-	-	-
Flag	0.15	3.223	-	-	-	-
Drift	0.09	3.313	-	-	-	-
CX3	0.15	3.463	- 7.1429	- 14.2857	-	-
Drift	0.55	4.013	-	-	-	-
CX4	0.15	4.163	7.1429	14.2857	-	-
Drift	0.145	4.308	-	-	-	-
Q4	0.10	4.408	-	-	-12.86	-13.5
Drift	0.15	4.558	-	-	-	-
Q5	0.10	4.658	-	-	+9.16	+9.63
Drift	0.15	4.808	-	-	-	-
Q6	0.10	4.908	-	-	+16.	+14.3
Drift	0.838	5.746	-	-	-	-

The orbit bump, as computed by the MAD program, is shown in Fig. 18. The correctors strengths have been computed by assuming ‘thin-lens’ approximations, i.e. considering the four correctors as pure horizontal kicks. This is a good approximation for thin magnets, as the three new correctors, but not suitable for the long dipole used as first corrector. Hence the corrector strengths will have to be adjusted during commissioning of the line, by looking at the beam position and shape at the flag located at the end of the transfer line. The quadrupole strengths were computed in order to match the beam phase space at the linac exit to the undulator beamline.

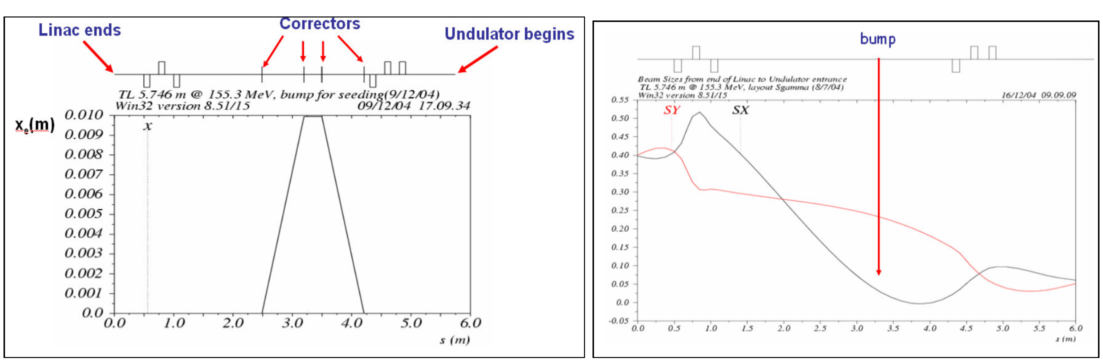

(a) (b)

Fig. 18. *MAD output (a) 10 mm bump (b) transfer line electron beam size in mm*

4.2. Bending magnets design and specifications

The chicane will be composed by the same bending magnet used to inject the beam into the dogleg (but operated with a lower magnetic field) and by three identical dipole magnets (see Fig. 19), which have been designed starting from the following data:

- Beam rigidity (for E = 200 MeV): $B\cdot\rho = 0.667$ T·m
- Max. deflecting angle: $\alpha = 10$ mm / 700 mm = 14.3 mrad
- Integrated B_{ver} field: $I_{z0} = B\cdot\rho\cdot\alpha = 9.53$ T·mm = 9530 Gauss-cm
- With $L_{dip} = 60$ mm $\rightarrow$ B = 0.159 T = 1590 Gauss
- Constraint: $B_{max} < B_{sat}$

The three corrector magnets have been designed in 3D by the code RADIA. Due to the short length of the dipole, fringing effects give a major contribution to the field integral and $B_{max} = 745$ Gauss is much lower than in the hard edge model (1590 Gauss). A shim of 2.5 mm was added on the external side of the gap, in order to reduce the asymmetry of Iz_0 vs. the transverse coordinate (see Fig. 20.b).

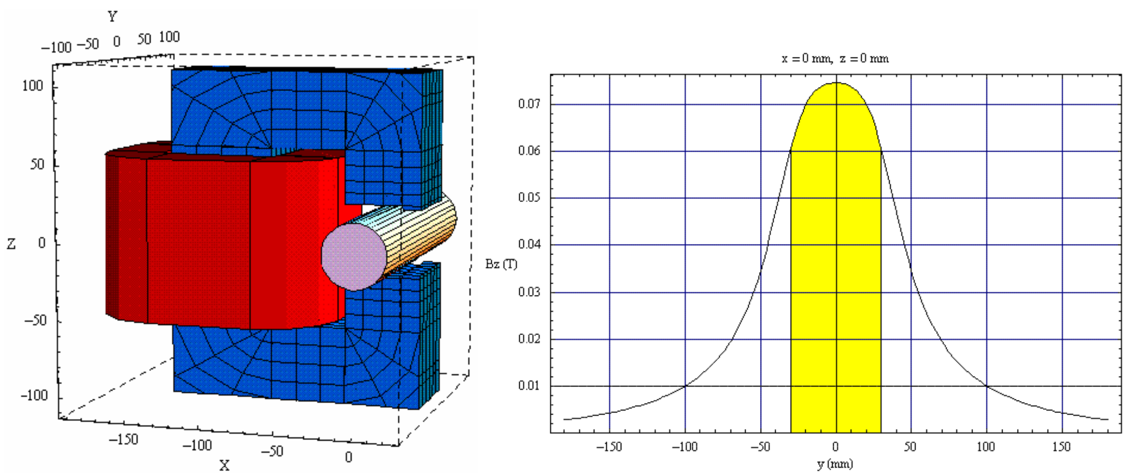

(a) *(b)*

Fig. 19. *(a) RADIA model of the corrector dipole, (b) Computed vertical magnetic field in the gap.*

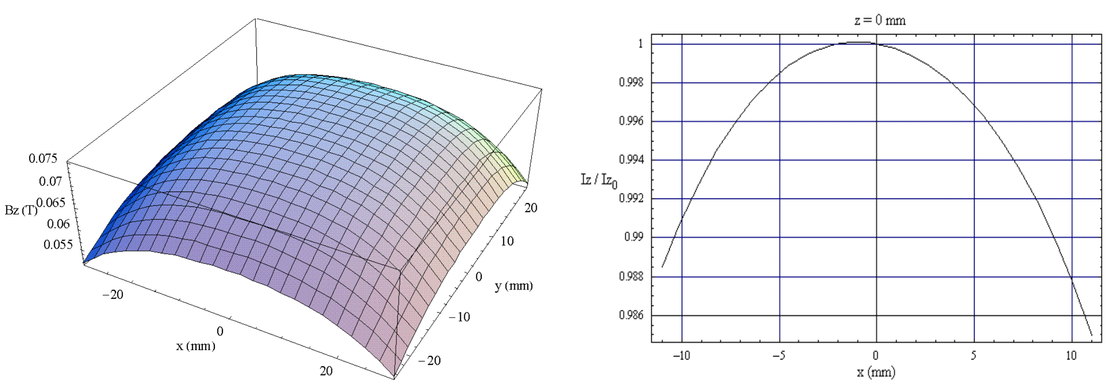

(a) *(b)*

Fig. 20. *(a) 3D map of the vertical magnetic field in the gap, (b) Integral of the vertical magnetic field along beam axis vs. the transverse coordinate, normalized to $Iz_0 = \int B_{ver}(0,y,0)dy$.*

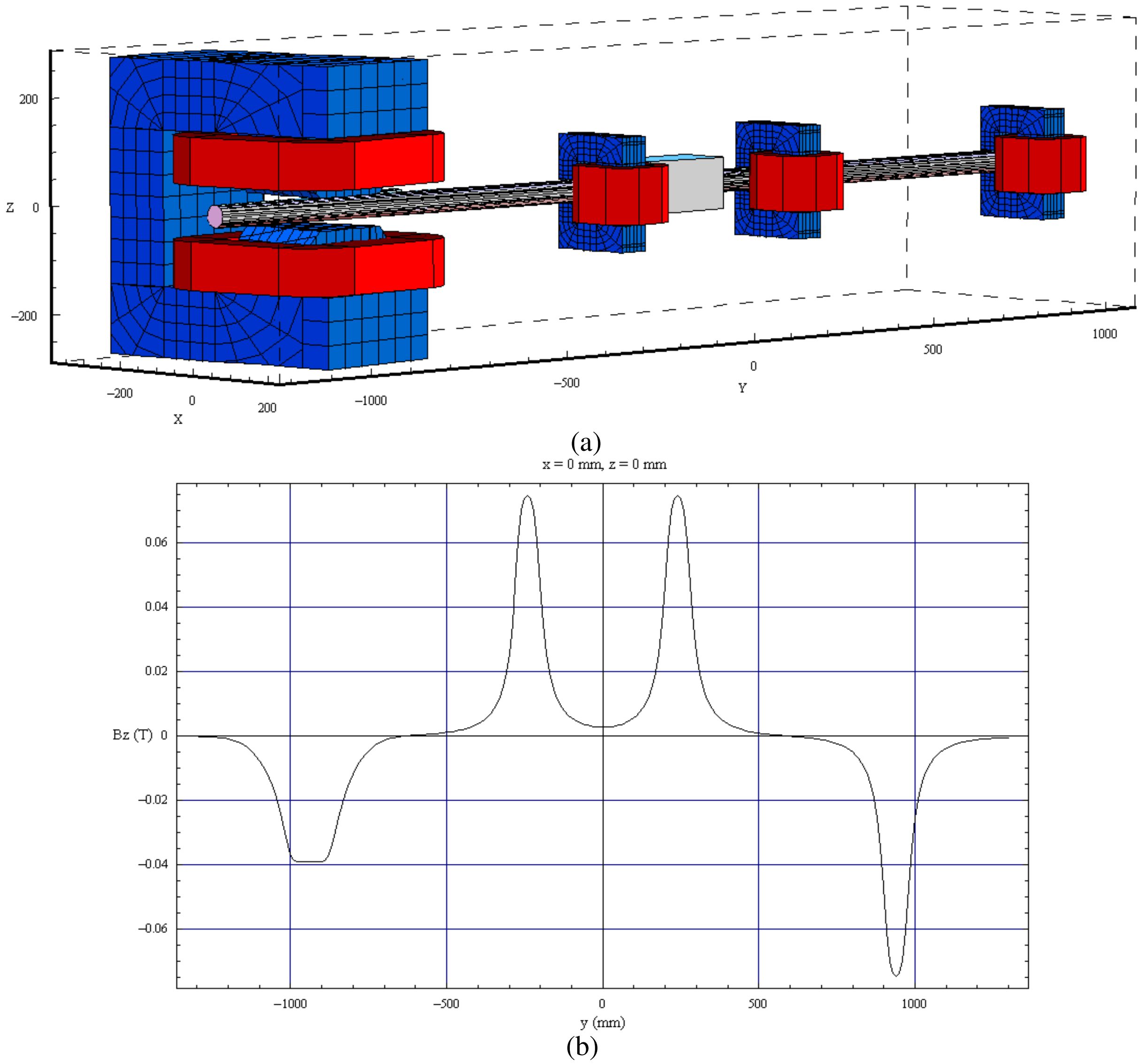

Fig. 21. *(a) RADIA model of the four dipole magnets of the chicane, (b) Computed vertical magnetic field along beam axis.*

In Tab. XIII and Tab. XIV the main parameters of the corrector magnets are shown. The regime temperature has been estimated assuming that all the power P is dissipated only by irradiation from the iron's free surface S: the Stefan-Boltzmann law $P/S = e\sigma\,(T^4 – T_c^4)$, with $e = 0.5$ and $T_c = 20°\mathrm{C}$, would give $T = 87°\mathrm{C}$. This value is certainly overestimated, as the power is mainly dissipated by convection, thus the regime temperature will be lower and water cooling should not be needed.

Tab. XIII. *Corrector dipole's parameters*

Length of iron yoke (y)	60 mm
Overall length	150 mm
Size of iron yoke (x × z)	170 mm × 217 mm
Aperture (gap)	47 mm
Height of poles (z)	50 mm
Width of poles (x)	50 mm

Shim's height (ext.)	2.5 mm
Coil size	40 mm × 107 mm
Total current	2894 A-turn
Current density (avg.)	0.676 A/mm2
Max. B field in iron	7160 Gauss
B field in the gap	750 Gauss
$Iz_0 = \int B_{\mathrm{ver}}\, dl$ on axis	9530 Gauss-cm
$\int B_{\mathrm{ver}}\, dl$ at –5 mm	9520 Gauss-cm (–0.15%)
$\int B_{\mathrm{ver}}\, dl$ at –10 mm	9450 Gauss-cm (–0.91%)

Tab. XIV. *Power consumption and heat dissipation*

Packing factor	65%
Effective copper area	2782 mm2
Number of turns	695
Wire dimensions	4 mm2 × 276 m
Wire resistance	1.21 Ω
Current per wire	4.16 A
Voltage drop	5.02 V
Dissipated power	20.9 W
Dissipating surface	0.078 m2
Regime temperature(*)	87°C

(*) assuming only irradiation: $P/S = e\,\sigma\,(T^4 - T_c^4)$ with $e = 0.5$ and $T_c = 20°C$

4.3. Beam dynamics simulations

Accurate beam dynamic simulations in the transfer line from the SPARC linac exit to the undulator have been done by using PARMELA code. As described in the previous paragraphs the transfer line includes two triplets of quadrupoles aimed to match the beam phase space parameters at the exit of the linac to the required values at the undulator entrance and a non-symmetric magnetic chicane deflecting the beam in the position of the mirror used for the injection of the seeding radiation in the FEL amplifier. The main aim of these computations was to control the effect of the chicane fields on the beam dynamics.

Due to the large aperture of the short dipole magnets of the chicane an accurate modelization of the magnetic fields of all the magnetic elements placed in the beamline based on 3D maps retrieved by RADIA code was preferred to the usual approach based on the hard edge model. In particular the maps of the single elements (quadrupole and dipole) on a grid x,y,z have been computed by RADIA and, since in our case the fringing fields overlap and PARMELA does not accept overlapping maps, an interfacing Fortran program was written that, starting from the single 3D maps, performs the sum of the overlapping fields and creates the input files describing the magnetic fields in the beam line for PARMELA.

The computations, that include the effect of beam space charge, were done for two beam energies, 155 and 200 MeV and two beam offsets, 5 and 10 mm.

The chicane magnetic fields must be set in order to get the desired beam deflection and contemporary to control the centroid position and angle at the undulator entrance that must be kept within the prescribed tolerances (respectively *100 μm* and *50 μrad*). As we will see in the following at this aim the four magnets must be powered independently.

In figure Fig. 22.a,b the setting of the magnetic fields of the chicane for a bump of 5 mm at an energy of 155 MeV are shown: the magnetic field on the first dipole is set to ~150 gauss in order to get the necessary deflecting angle of 7.14 mrad while the magnetic fields of the inner dipoles must be equal (~300 gauss) in order to get a null angle in the middle while a magnetic field of opposite sign on the fourth dipole (in first approximation equal to the magnetic fields of dipoles 2 and 3) reports the beam on the axis. In the two figures the resulting evolution of the centroid angle and position is shown.

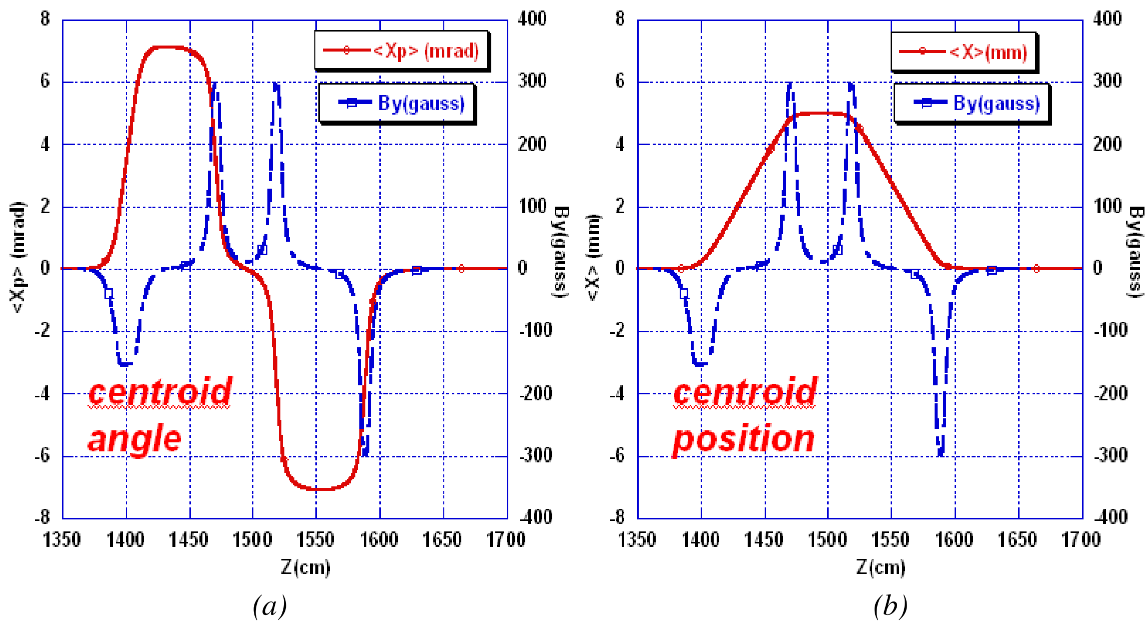

Fig. 22. *Computed centroid motion in the chicane: (a) centroid angle (b) centroid position. In both cases the curves corresponding to the chicane magnetic fields are superimposed.*

If we double the magnetic field values of the previous setting we obtain a doubled bump of *10 mm*, but a residual centroid angle of *273 μrad* and a centroid displacement of *50 μm* appear. This is due to the non-uniformity of the magnetic field in the dipole gap that decrease going from the centre to the external . This effect can be corrected increasing of 1% the excitation on the inner dipoles (#2 and #3) respect to the dipole #4, that is sufficient to get a zero field integral and correct the output angle and position.

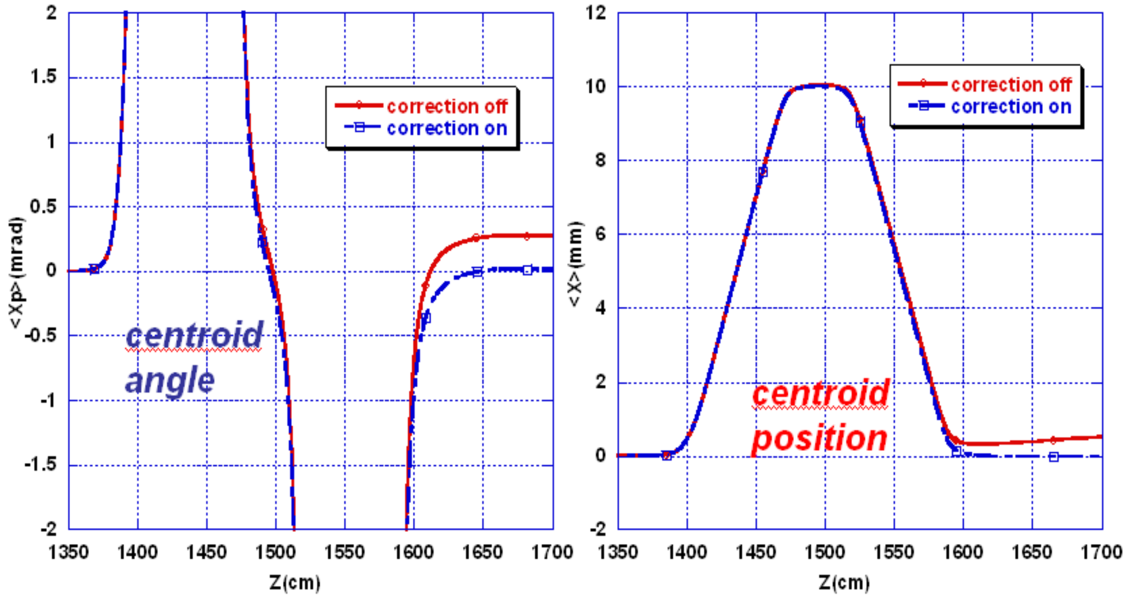

(a) *(b)*

Fig. 23. *(a) centroid angle (b) centroid position with and without the correct unbalancing of the last three chicane-dipoles magnetic fields*

The above setting was done switching off the last triplet of quadrupoles placed before the undulator. When we switch on all the quadrupoles we observe that, due to the overlapping of the fringing fields of the last chicane dipole and the first quadrupole of the second triplet a further correction of 0.5% on the excitation of the last dipole magnet is necessary to force the residual angle error within the tolerances.

In Fig. 24 we can see the beam spot evolution in the chicane: in the point of the maximum displacement the whole beam spot is less than 3 mm. In figure 4 the horizontal and vertical envelopes are shown. The same criteria have been used for the setting of the magnetic fields for a bump of 10 mm at 200 MeV (Fig. 26): a magnetic field of 400 gauss is necessary on the first chicane dipole while less than 800 gauss is required in the following three dipoles.

As to the emittance PARMELA gives, for a bump of 10 mm at 155 MeV, a growth of ~3% in the bending plane due to a residual dispersion given by the combined effect of the space charge and the motion in the bending magnets. This emittance growth decreases to ~0.7 % for a bump of 10 mm at 200 MeV. The amount of emittance growth in both cases can be considered negligible.

As to the mismatching parameter defined as $\xi = \frac{1}{2}\cdot\left(\beta_0\gamma - 2\alpha_0\alpha + \gamma_0\beta\right)$ where the label *0* corresponds to the perfectly matched parameters, PARMELA gives ξx=1.0984, ξy=1.0683 at 155 MeV and ξx=1.0983, ξy=1.099 at 200 MeV that are well within the tolerances.

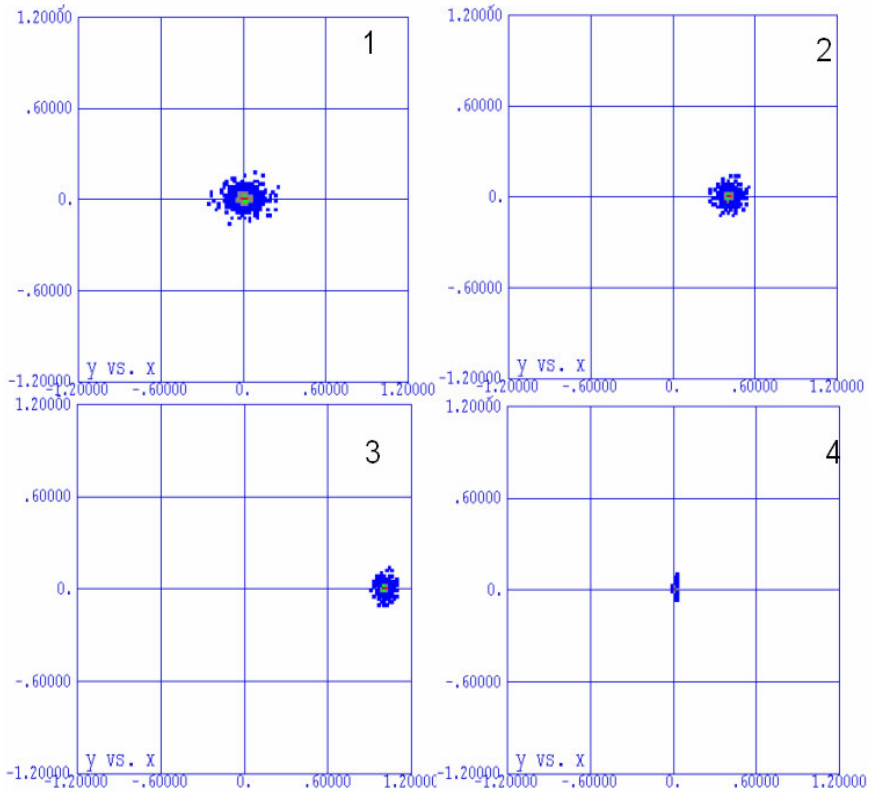

Fig. 24. *PARMELA output: beam spot in 4 different longitudinal position in the chicane. All the measures are in cm. The beam energy is 155 MeV*

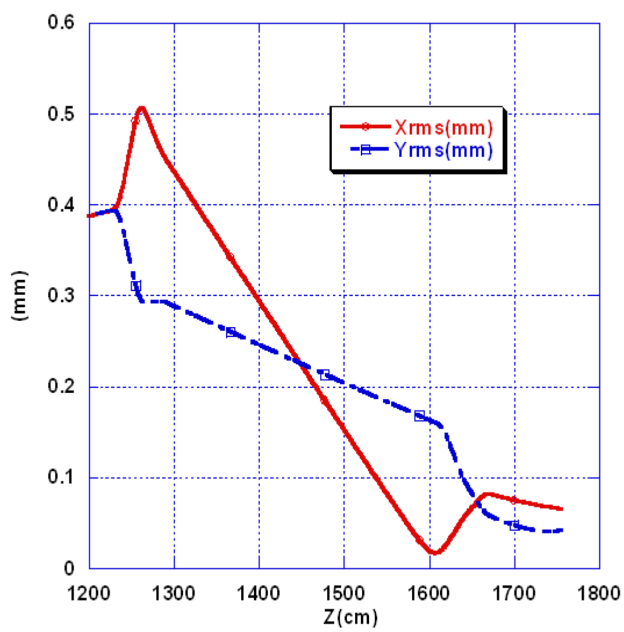

Fig. 25. *Horizontal and vertical envelopes in the beam transfer line as computed by PARMELA. The beam energy is 155 MeV.*

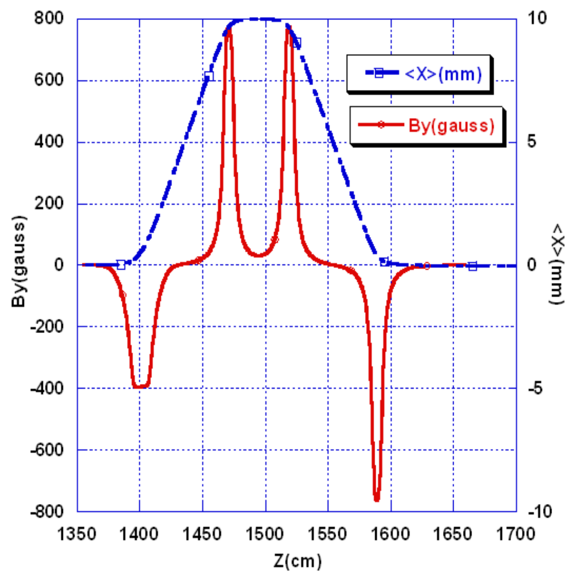

Fig. 26. *Chicane magnetic field setting and centroid displacement for a bump of 10 mm at 200 MeV*

In conclusion the results of the study performed by PARMELA show that the injection scheme based on the use of a chicane in the SPARC transfer line for the seeding experiment does not give great problems in terms of beam emittance and phase space matching at the entrance of the undulator. However a special care must be given to avoid undesirable effects on centroid position and angle at the entrance of the undulator due to the perturbation introduced by the chicane.

4.4. Wake fields at the injection mirror

The magnetic chicane deflects the electron trajectory from the straight path of a distance comprised between 5 and 10 mm. In this section the effects of the interaction of this beam with the last mirror inserted in the straight path is analysed.. The geometry of the system is shown in Fig. 27. The mirror is modelled as a conducting block located at 1 cm of offset from the pipe axis (assumed circular with radius b = 2 cm), and the mirror, tilted by 45°, is 6 mm large and 20 mm long. At the bottom of the pipe there is a hole to allow the seed laser to enter in the chamber.

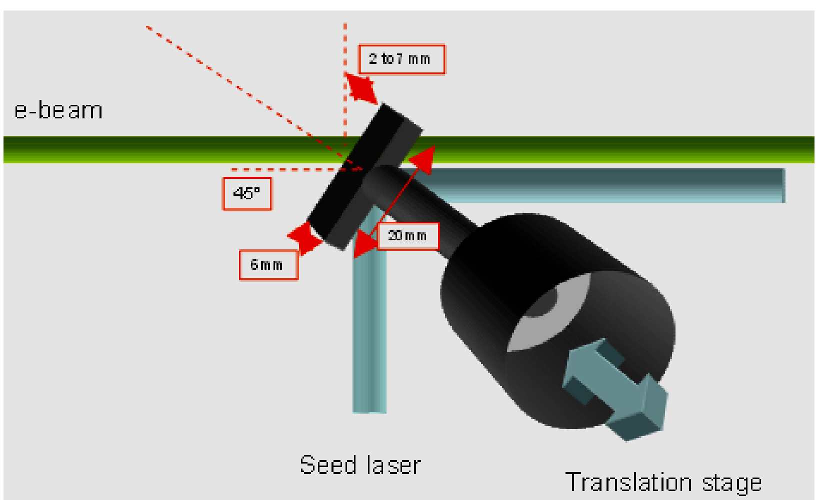

Fig. 27. *Last mirror layout.*

As a first evaluation of the wake fields, the whole system has been replaced by a pill box cavity with a gap g = 10 cm. Since the pipe cut off frequency is much lower that the bunch length (σ_z = 1 mm), the diffraction theory can be used to obtain the wake fields[45][44]. Furthermore it can be verified that if the cavity radius d is larger than ~ 4 cm, the so called cavity like regime is satisfied [46]:

$$g < \frac{(d-b)^2}{2\sigma_z} \tag{4}$$

The physical meaning of the above expression is that the time necessary to the generated electromagnetic field to reach the cavity walls and to act back on the bunch is longer than the transit time of the bunch. In this situation the wakes do not depend on the cavity radius and can be written as

$$W_{\parallel}(z) = -\frac{Z_0 c}{\sqrt{2}\pi^2 b}\sqrt{\frac{g}{z}} \quad \left(\frac{\mathbf{V}}{\mathbf{C}}\right) \tag{5}$$

$$W'_{\perp}(z) = \frac{2^{3/2} Z_0 c}{\pi^2 b^3}\sqrt{gz} \quad \left(\frac{\mathbf{V}}{\mathbf{C\,m}}\right) \tag{6}$$

with Z_0 the vacuum impedance and c the speed of light. The minus sign in the longitudinal wake indicates lost energy, and the transverse wake field is per unit of displacement.

By assuming a longitudinal Gaussian distribution, it is possible to calculate the longitudinal and transverse wake potentials that represent respectively the energy lost by a particle and the transverse momentum deflection due to the whole bunch. Since the cavity has cylindrical symmetry, the wake potentials for the Gaussian bunch have also been calculated with ABCI code [47]. The results are shown in Fig. 28. The analytical estimations are in good agreement with the code calculations, and since the first ones are in any case more pessimistic, they have been used to evaluate the effect on the beam dynamics.

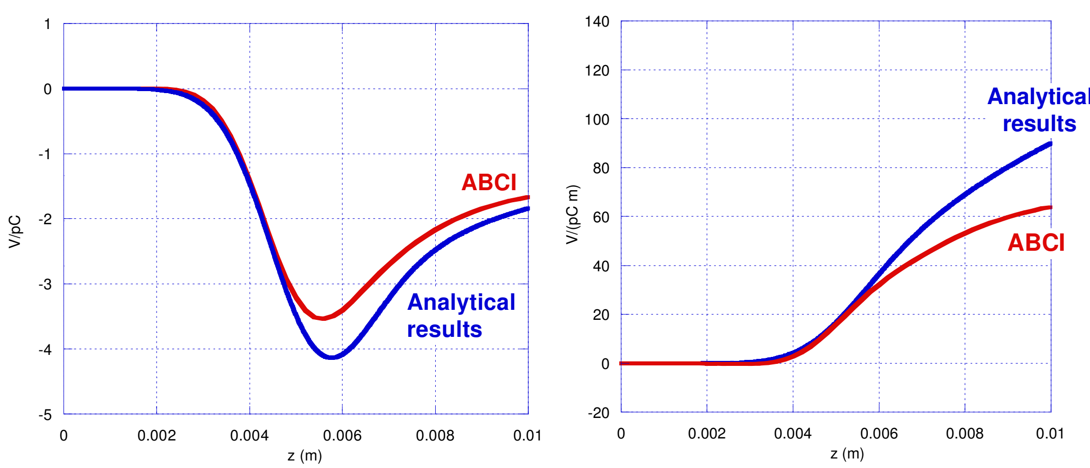

Fig. 28. *Longitudinal and transverse wake potentials for the pill box cavity.*

In the longitudinal case, the obtained loss factor is *2.93 V/pC* and the energy spread is *1.18 V/pC*. For a 1 nC bunch charge and 150 MeV these results give a relative loss of 2 x 10^{-5} and a relative energy spread of 8 x 10^{-6}. In the transverse case, by considering the simplifying hypotheses that the wake acts as a Dirac Delta function in the longitudinal coordinate and the bunch has negligible transverse dimension and enters the cavity with zero divergence, at 1 cm off axis it gets a divergence of about 10^{-6} rad. The effect of the mirror has been evaluated with MAFIA code in time domain [48]; 3D simulations were necessary because of the 1 cm off set of the bunch. The model of the structure is shown in Fig. 29. Due to mesh limitation, the mirror, sustained by a vertical support, is perpendicular to the pipe axis and the cavity is absent.

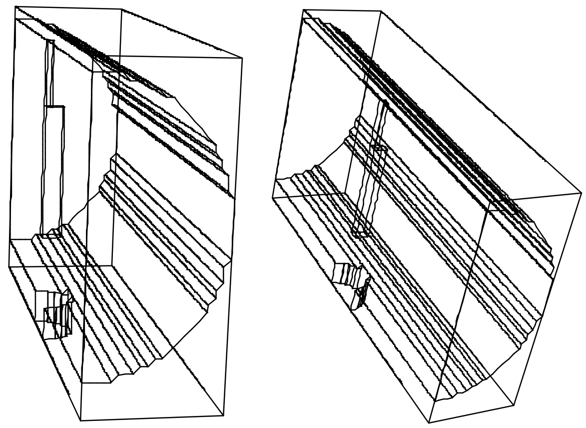

Fig. 29. *MAFIA model of the structure.*

The resulting longitudinal and horizontal transverse wake fields are shown in Fig. 30. The vertical transverse wake is negligible because in this plane the asymmetry is small and the bunch is symmetric with respect to the pipe. The horizontal transverse wake is in V/C since it is not linear with the transverse displacement due to the non symmetry of the system. By comparing Fig. 30 and Fig. 28, it is possible to note that the longitudinal wake is about a factor of 2 lower than that produced by the cavity alone. The case of the transverse wake is different: it is important to point out that to compare the wakes, Fig. 30 must be multiplied by the bunch off set (1cm). As a consequence the kick received by the bunch is about a factor 2 higher in the case with the mirror.

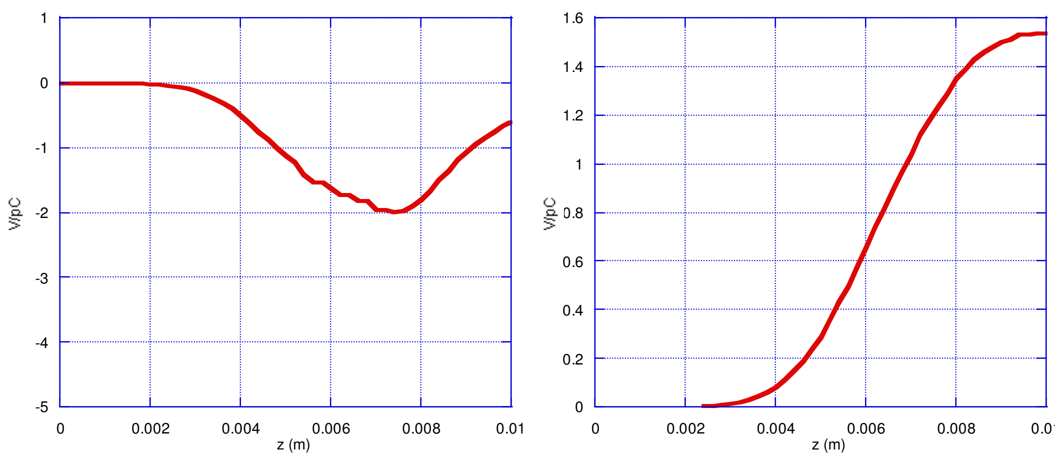

Fig. 30. *Longitudinal and transverse wake potentials of the last mirror*

All the results show that the wake field effects on the beam dynamics can be neglected.

5. Harmonic Generation system

5.1. Introduction

The design of the harmonic chamber and its implementation in the SPARC facility is here discussed. Different criteria are taken into account such as the performances of the high harmonics in gases, the vacuum needs, the resistance of the optics in the transport line, the geometrical constraints due to the accelerator and the building. Diagnostics and experimental procedure are also discussed.

The system consists of two chambers. The generation of harmonics in gas occurs in the first chamber, and the VUV beam adaptation for its overlap with the electron beam takes place in the second chamber. A final vertical periscope is used to align the VUV beam in the undulator. This first version concerns the harmonic number 5, at 160 nm. It seems better to optimize everything at one given wavelength with the best optics and the maximum available intensity of harmonics, in order to put all the chance of rapid success, and make systematic studies. Then, once the experimental procedure and the behaviour versus different parameters is better understood, we can proceed to experiments at different wavelengths, by changing the mirrors.

5.2. Description of the harmonic chamber in the general implementation

The general implementation of the production of the harmonics in gas is described in Fig. 31. From the laser hutch, the IR laser is sent in the first chamber, located behind the pillar (cf scheme of the SPARC hall), at typically 1.5 meters of the second chamber, which is used as a harmonic generator. We first consider using a gas jet. The two chambers are centered at 80 cm from the floor, in order to allow turbo molecular pumps to be installed on the vertical axis of the chambers, in the lower position, for insuring a good mechanical stability. A two chamber system has been chosen, since it separates the functions of harmonic generation and spectral and mode adjustments. Indeed, it makes the vacuum system much easier, and the pumping is more efficient. In the first chamber, a level vacuum of 10^{-3} mbar is expected, with a turbo-molecular pump. A vacuum duct of small diameter connecting the two chambers, with a length of two meters, allows differential pumping to take place. Besides, a transparent valve with CaF_2 or doped SiO_2 or MgF_2 or LiF plate is used to isolate the vacuum between the two chambers, letting the VUV radiation of the harmonics goes through. One considers 1.5 meters from the e-beam line to the middle of the second chamber and another 1.5 meters to the middle of the first chamber. The distance between the first chamber and the focusing lens of the IR laser in the gas jet is assumed to be 2 m. Let’s point out that the energy (2.5 mJ) implies to employ a rather short focal length.

The second chamber is located closer to the chicane entrance. It serves for the harmonics mode adaptation for a correct overlap with the electron beam in the modulator. Spectral selection can be added, even though the spectral width of the FEL gain (0.1%) should be sufficient. Further elimination of the IR laser could also be necessary. Finally, a last X shape chamber comporting the second periscope mirror is installed at the entrance of the chicane.

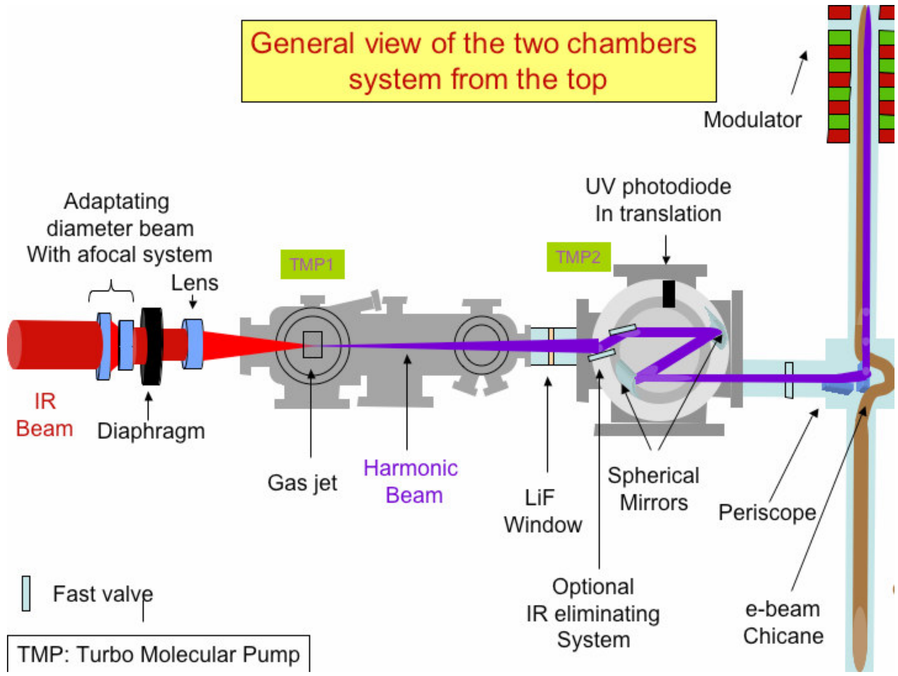

Fig. 31. *Lay-out of the harmonic chamber for the seeding experiment at SPARC. The first chamber is dedicated to the production of harmonics in gas. The second chamber is required for the opical mode adaptation.*

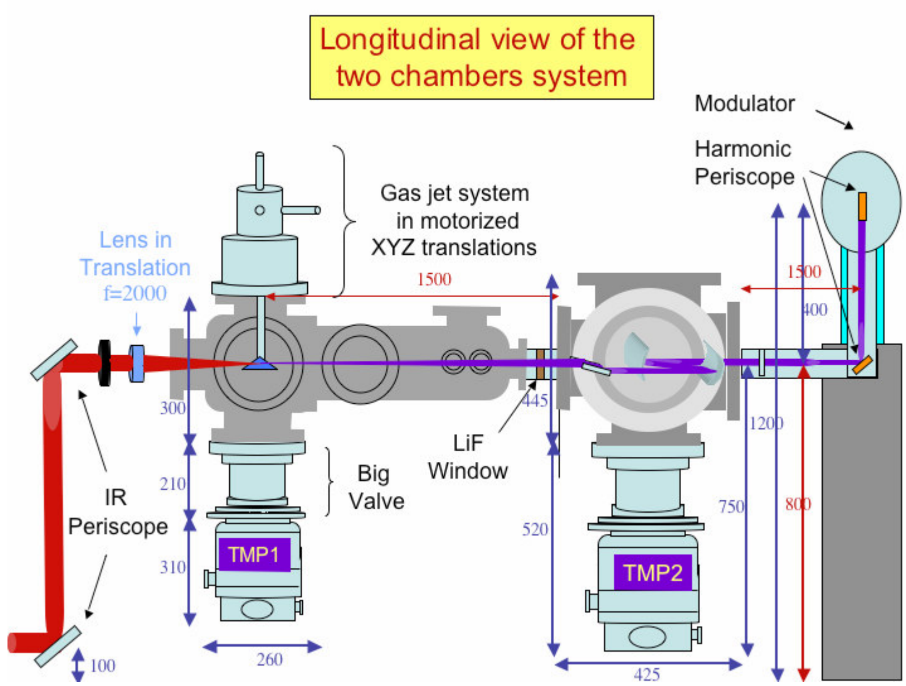

Fig. 32. *As in Fig. 31, lay-out of the harmonic chamber for the seeding experiment at SPARC – Lateral view.*

5.3. The first chamber : harmonic in gases

Typically, a laser energy per pulse of 2.5 mJ in 100fs should provide more than 5 nJ of harmonics intensity at 160 nm with 2 m focal length[49].

In the laser hutch, a motorized delay line employed for the synchronisation between the electron bunch and the optical light will be installed. Then, the IR laser exits the laser hutch, is sent in a periscope. Two lenses will be employed to adapt the size of the infra-red beam, which will be further changed with a set of iris. Finally, the beam is focussed in the gas jet. According to the distance of implementation, the complete calculation of the light beam transport can be carried out. A first estimation would give a focal length of 2 m and a beam diameter of 15 mm for a focused beam of 100 µm in the jet. Such a focal value is chosen for optimising the conversion rate in gas, for enhancing the waist at the focalisation point and decreasing the harmonic divergence. This lens should be mounted on a translation table, so that the position of the waist of the laser can be adjusted and the harmonics can be optimised. The polarisation of the IR laser should be horizontal.

A diameter of the infra-red beam of D=15 mm on the 2 m focal length lens allows $8*10^{13}$ W/cm^2 (close to the conversion saturation) to be produced at the interaction region with 2.4 mJ of incident energy.

The gas jet system should be mounted on a mechanical holder allowing XYZ translations. The final choice between gas jet and cell is not yet definite, but the same holder could be used and adapted for one or the other. A visualisation of the cell entrance window could be adapted eventually.

A level vacuum of 10^{-3} mbar is expected, and a strong turbo-molecular pump is selected (Alcatel ATH1300M, 1300 l/s for N_2, He, H_2), which will be located below the chamber for stability reason. This defines the minimum height of the harmonic beam, i.e. 80 cm from the floor.

Then, the harmonics are sent in a vacuum duct. It is connected to the first chamber with a transparent valve, letting the harmonics go through but isolating the vacuum of the first chamber. One expects a transmission of 70% (resp. 7%) at 120 nm with a LiF window (Crystan) for a thickness of 100 µm (resp. 3 mm). One should be careful with birefringence. Further Infrared coating can be added. The diameter of the plate should be smaller than 10 mm.

5.4. The second chamber : waist adaptation

The second chamber includes two spherical mirrors for adapting the waist of the VUV. There is still some concern about the spectral selection and the elimination of the IR laser. On one hand, the spectral bandwidth of the gain is very narrow, and the IR can not exchange energy with the electron beam. This has been confirmed by simulations done in ref.[50]. Second, one should be sure that the intense IR beam will not damage the optics, used for the mode shaping. Before of the possible change of the refractive index of materials deposited by evaporation under vacuum, multilayer mirrors made with ion beam assisted techniques or sputtering can be used. In such a case, the resistance to intense laser radiation is significantly increased. In the case of lens presented below (2 m focal lens), one expects 11mJ/cm2 (M^2=1.5) at 1 meter of the gas jet. Such a fluence is not very important. So, such a value is still acceptable with evaporated mirrors (private communication A. Gatto). In consequence, we consider here not to implement here infra-red rejection with the help of two reflecting plates. We could probably employ well designed multilayers for H5, which will eliminate the infra-red. This will be further discussed with optical manufacturers in the near future. Besides, one can prepare a removable vertical plate transmitting H5 and eliminating the IR, so that tests can be done with and without the infra-red.

The harmonics beam is sent in a system of two concave mirrors reflecting at 160 nm at nearly normal incidence, for adapting the waist in the middle of the modulator. These mirrors will be produced by fluoride multilayers, and one expects reflectivities of the order of 95%. The two spherical mirrors should be installed on specific mirror mounts, adapted for the vacuum environment. Besides, the fine tilt tuning will be ensured by piezo motors. Two additional translation stages should be added on the first and the second spherical mirror, for the adaptation of the focusing point in the undulator. The infra-red reflectivity of a multilayer mirror from Fraunhoffer Inst. (Jena) of mirrors at 160 nm is of 6%. It means that the use of the fourth mirrors leads to an infra-red attenuation of 1.3 10^{-5}.

The vacuum is insured with another turbo-molecular pump allowing to obtain 10^{-6} mbar. The expected vacuum in the undulator is 10^{-8} mbar. So, some adding differential pumping must be done.

5.5. The chamber of the periscope

The harmonics beam is sent in the undulator with the help of a vertical periscope, bringing the beam from a 80 cm height to 1.2 m, which is the level of the electron beam. The chamber for these two mirrors should be further designed, according to precise drawings of implantation of the first two chambers and of the environment of the chicane (available space and the design of the vacuum duct at this point). One could think of a specific X shape chamber. The two mirrors of the periscope are also fluoride multilayers, at 45° incidence. The adjustment of the vertical and horizontal tilt of these two mirrors should be remote controlled.

5.6. Optics

5.6.1. IR and VUV beam transport

The calculation of the IR evolution allows the evaluation of the waist size on the gas jet and the determination of the harmonic generation process, the estimation of the energy density of the IR beam hitting the optics (a threshold of beyond 100 mJ. cm^{-2} should not be overcome) or occurring in air, which could lead to phase self-modulation destroying the beam Gaussian distribution. Besides, the harmonic beam propagation is crucial for evaluating the overlap between the light wave and the electron bunch in the modulator.

The propagation formulas used here are those of a non-purely Gaussian mode, that is to say with the M^2 Gaussian quality factor of a beam. M^2 is equal to 1.5 for the IR beam. The harmonic beam consisting of H_{2q+1} harmonics is also Gaussian with M^2 ($(2q+1)^{th}$ harmonic) = M^2 (IR)*$q^{0.5}$. In fact, the waist and pulse duration of the harmonic beam can be deduced from the IR ones, by dividing with $q^{0.5}$. So, for H_5, M^2 is equal to 2.1 ($1.5*2^{0.5}$), its waist and pulse duration are respectively 72 µm and 72 fs.

The evolution of the transverse size of the beam, w_p (Z) as a function of the longitudinal coordinate Z, is given by equation (7)

$$w_p(Z) = w_o \times \sqrt{1+\left\{\frac{Z}{Z_R}\right\}^2} \qquad (7)$$

with

$$Z_R = \frac{4M^2\lambda f_\#^2}{\pi} \qquad (8)$$

or

$$Z_R = \frac{\pi . w_0^2}{M^2\lambda} \qquad (9)$$

We introduce the parameter

$$f_{\#} = \frac{f}{D} \tag{10}$$

which defines

$$w_0 = \frac{2M^2 f_{\#} \lambda}{\pi} \tag{11}$$

with w_0 the laser waist, Z_R the Rayleigh range, λ the radiation wavelength (i.e. e. 800 nm), and $f_{\#}$ the f-number (number of opening), D the diameter of the beam before focusing and f the focal length. The beam divergence θ_D I given by:

$$\theta_D = \frac{M^2 \lambda}{\pi w_0} \tag{12}$$

The harmonic beam propagation is modified by the two SM_1 and SM_2 spherical mirrors, as illustrated in Fig. 33. After the first lens focusing the IR beam in the gas jet or cell, the two spherical mirrors SM_1 and SM_2, which readjust the focusing of the high harmonic beam, are considered as converging lenses of focal length f_1 and f_2. As the spherical mirrors are regarded as lenses of f focal length, in the paraxial approximation, the characteristics of the transmitted beam become:

$$s' = f \times \left[1 + \frac{\left(\frac{s}{f} - 1 \right)}{\left(\frac{s}{f} - 1 \right)^2 + \left(\frac{Z_R}{f} \right)^2} \right] \tag{13}$$

$$w_0' = m \times w_0 = \frac{w_0}{\sqrt{\left(\frac{s}{f} - 1 \right)^2 + \left(\frac{Z_R}{f} \right)^2}} \tag{14}$$

with s (resp. s') the object (resp. image), w_o' the image waist and Z_R' the image Rayleigh range. The coefficient m is the factor of enlargement of the lens. Indices 1 and 2 are used respectively for SM_1 and SM_2.

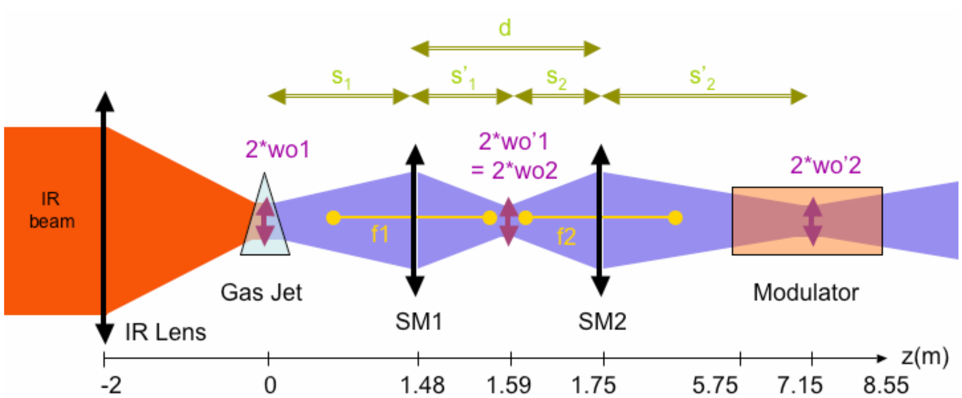

Fig. 33. *Longitudinal evolution of the IR and harmonic beams in transversal domain. w0 and w0' are respectively the laser object and image waists at the focusing points. The parameters s and s' are the laser object and image distance respectively.*

Tab. XV presents the results of the IR propagation in the transversal domain until the focusing position in the gas.

Tab. XV. *IR beam (800 nm, 100 fs) calculation : Waist evolution along the local coordinate Z. Case of a 2 m focal length f, a diameter of 15 mm on the lens, a waist at the focussing point W_o = 102 µm, Z_o=27 mm, Guassian factor M2=1,5 E_{laser}=2,44 mJ and f#=133 for an intensity near the focalisation point around I=8 10^{13} W/cm^2.*

location	Z	Wp(Z)	Fluence	Power density
	m	µm	J/cm2	W/cm2
Focalisation lens	-2	7501	0,003	2,76E+10
	-1,78	6676	0,003	3,49E+10
	-1,6	6001	0,004	4,32E+10
	-1,5	5626	0,005	4,91E+10
	-1	3751	0,011	1,11E+11
	-0,75	2814	0,020	1,96E+11
	-0,5	1878	0,044	4,41E+11
	-0,25	943	0,175	1,75E+12
	-0,2	757	0,272	2,72E+12
	-0,15	572	0,476	4,76E+12
	-0,13	498	0,627	6,27E+12
	-0,1	389	1,030	1,03E+13
	-0,08	317	1,550	1,55E+13
	-0,06	247	2,550	2,55E+13
	-0,04	181	4,732	4,73E+13
	-0,03	152	6,754	6,75E+13
	-0,025	138	8,117	8,12E+13
	-0,02	126	9,722	9,72E+13
	-0,015	116	11,489	1,15E+14
	-0,01	109	13,203	1,32E+14
Gas output wo1	0	102	14,992	1,50E+14

The harmonic beam propagation is calculated according to the spherical mirrors characteristics given in Table 2, which are determined by the IR lens ($w_{o1harmonic}=w_{01\ IR}/2^{0.5}$=72 µm), the overlap in the undulator with the e-beam ($w_o'_2$= 277 µm) and the geometry of the chamber.

Tab. XVI. *Spherical mirror characteristics used for the harmonic beam transport, d being the distance between the two spherical mirrors. a) Chosen values, b) deduced values from eq. (7) to (14). Re=R.cos(θ) is the equivalent radius of curvature with R the radius of curvature and θ the incidence degree on a spherical mirror*

	wo1	s1	f1	f2	d	s'2	wo'2
Unit	µm	m	m	m	m	m	µm
Value	72	1.62	0.0749	0.0749	0,1543	6,02	277

(a)

	i	s_i	Re	R	θ	Z_{Ri}	w0i	s'i	wo'i	ZR'i	M2	d
Unit		m			degree	m	µm	m	µm	m		m
Value	1	1.62	0,15	0,15	5	0,034	72	0,0785	4	0, 00008	3	0,1543
Value	2	0,0758	0,15	0,15		0,00008	4	6,02	277	0,505		

(b)

Tab. XVII gives the characteristics of the optical beam along its longitudinal coordinate Z starting from the harmonic generation location and as long as it propagates towards the undulators.

Tab. XVII. *Harmonic beam propagation for a wavelength of 160 nm. M2=3. Local Z represents the longitudinal coordinate with its origin centered at each focusing point.*

Location	Z	Local Z	Wp (Z)	H5 Energie	Power
	m	*m*	*µm*	*nJ*	*kW*
Gas output Wo1	*0,00*	*0*	*72*	*5,00*	*69,4*
	0,10	*0,1*	*224*	*5,00*	*69,4*
	0,25	*0,25*	*536*	*5,00*	*69,4*
	0,50	*0,5*	*1064*	*5,00*	*69,4*
	1,00	*1*	*2124*	*5,00*	*69,4*
Optional SiO2 plates	*1,47*	*1,47*	*3126*	*2,50*	*34,7*
First spherical mirror	*1,62*	*-0,08*	*3444*	*2,00*	*27,8*
	1,66	*-0,04*	*1776*	*2,00*	*27,8*
Wo2	*1,70*	*0*	*3*	*2,00*	*27,8*
	1,75	*0,05*	*2171*	*2,00*	*27,8*
Second spherical mirror	*1,78*	*-6,02*	*3333*	*1,60*	*22,2*
	2,00	*-5,79*	*3210*	*1,60*	*22,2*
	3,00	*-4,79*	*2661*	*1,60*	*22,2*
First flat mirror	*3,40*	*-4,39*	*2442*	*1,28*	*17,8*
	3,60	*-4,19*	*2333*	*1,28*	*17,8*
Second flat mirror	*3,80*	*-4,00*	*2223*	*1,02*	*14,2*
	5,10	*-2,69*	*1513*	*1,02*	*14,2*
Undulator entrance	*6,40*	*-1,4*	*821*	*1,02*	*14,2*
	6,80	*-1*	*617*	*1,02*	*14,2*
	7,20	*-0,6*	*432*	*1,02*	*14,2*
	7,60	*-0,2*	*298*	*1,02*	*14,2*
Undulator center	*7,80*	*0*	*277*	*1,02*	*14,2*
	8,50	*0,7*	*475*	*1,02*	*14,2*
Undulator output	*9,20*	*1,4*	*821*	*1,02*	*14,2*
	9,70	*1,9*	*1085*	*1,02*	*14,2*

plots the transversal waist versus its longitudinal position. One clearly sees the three changes of waists corresponding to first the IR focusing lens, and to the two focusing mirrors SM_1 and SM_2. The high harmonic beam is in fact focused at Z=7.8 m, corresponding to the centre of the modulator.

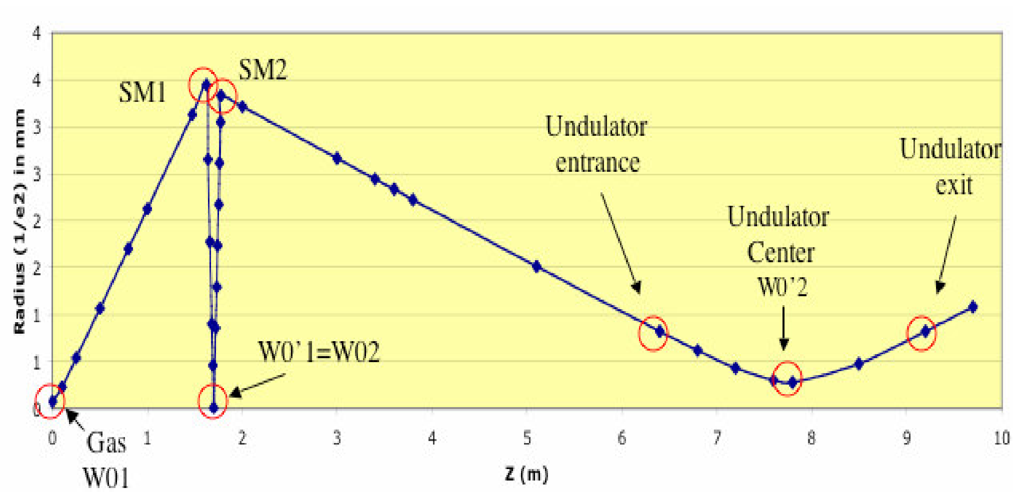

Fig. 34. *Longitudinal evolution of the transverse harmonic beam size.*

The transverse overlap with the electron beam can be estimated. The electron beam propagation is calculated using the following model. The e-beam size (Σ_X) can be calculated at this position using:

$$\Sigma_X = \sqrt{\left(\frac{\beta_X \varepsilon}{\gamma}\right)} \tag{15}$$

β is the beta function, ε is the emittance and γ the normalized energy. The e-beam divergence Σ_X' can be calculated too using the same parameters:

$$\Sigma_X' = \sqrt{\varepsilon_n / \beta_X} \tag{16}$$

The evolution of the waist inside the modulator can be deduced using:

$$W_e(Z) = 2 * (\Sigma_X + Z * \Sigma_X') \tag{17}$$

compares the e-beam and the harmonic beam evolutions, for an emittance of 2 π mm.mrad and a relativistic factor γ=411 (210 MeV). The electron and harmonic beams are focused at the centre of the undulator and with a similar waist, whereas the divergence of the two beams is different.

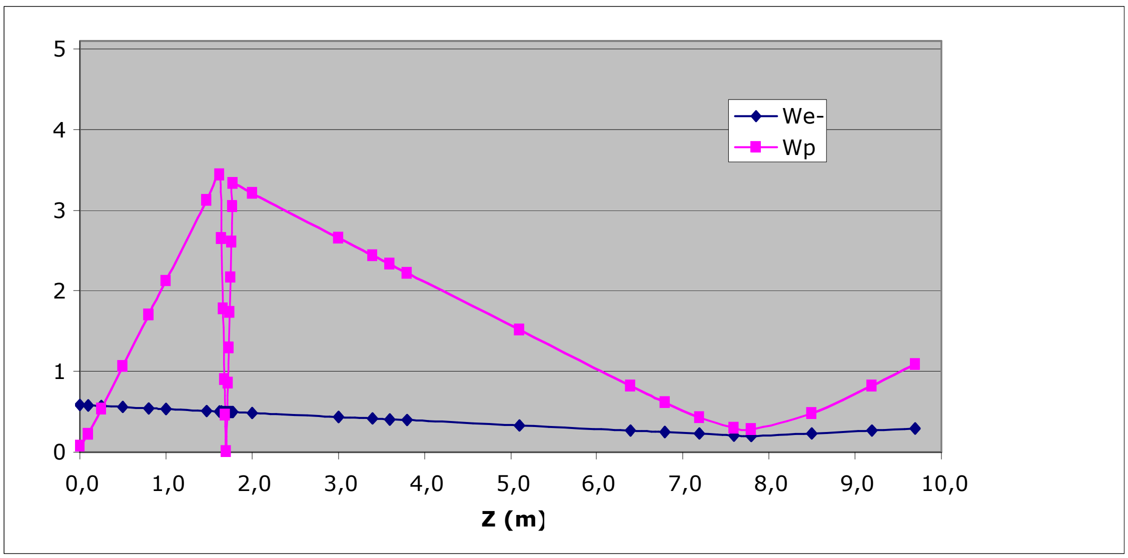

Fig. 35. *Longitudinal evolution of the transversal electron beam size in x and in y (W_{eX} and W_{eY}) and harmonic beam size (W_P), from the entrance of the modulator to its exit, for a focusing at the centre of the undulator.*

As the overlap is a crucial point for the seeding experiment, a detailed study of the effects of the focusing position along the modulator must be made. The first spherical mirror could provide some variations of focusing position and waist, in order to improve the overlap, if it is translated changing the s_2 value. In order to evaluate the tolerances relative to these adjustments, further simulations have been made.

5.6.2. Optics performances at 160 nm

Two strategies can be adopted. The reflective mirrors can either present a wide bandwidth in order to cover several harmonics, or they can be optimised for a specific wavelength.

In the first case, one should employ wideband mirrors, such as Al coated with MgF_2, in order to ovoid the oxidation. Reflectivity is 85% in the 200-800 nm range [51]. In the second case, one design λ/4 multilayers with adapted materials for this spectral range. The transmission of the materials in thin layers conditions is given in Fig. 36 [52].

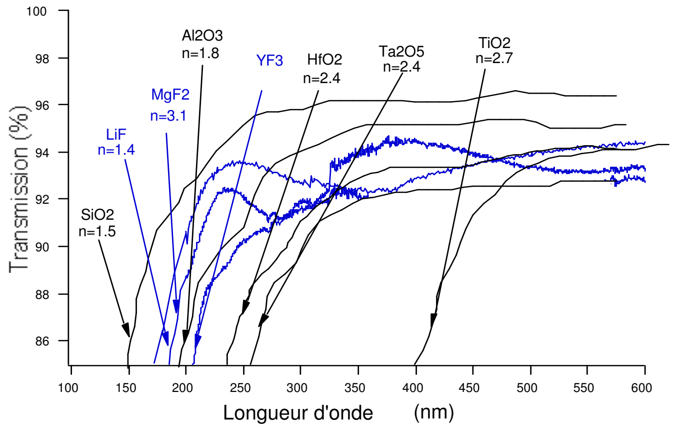

Fig. 36. *Limit of the transmission zone for different materials used in thin films multilayers*

An example used in Saclay, from BFI Optilas, provides 91% of reflectivity at 150 nm, and 10% at 800 nm for a mirror designed at 45°. Mirrors proposed by Fraunhoffer Institute offer a reflectivity in the infra-red of 6%. For example, with 4 mirrors of this type (the two spherical mirrors and the two mirrors of the periscope), the IR will be attenuated by five orders of magnitude). Further discussions with manufacturers will be reported.

5.6.3. Anti reflecting coatings at 800 nm

In Saclay, the reflecting coating is a silica plate coated with 3 double layers of SiO_2/TiO_2 at 10° incidence, manufactured by Fichou. Properties of normal incidence are under discussions.

5.7. Experimental Alignment procedure

Initially, the infra-red laser should be aligned on the magnetic axis of the undulator, which defines the axis of the interaction between the harmonics and the electron beam.

First, the infra-red laser, partially transmitted in the VUV optics is sent in the undulator. The two mirrors of the periscope are then used so that the infrared radiation should exit from the undulator. The IR light can be reflected or diffracted in the vacuum chamber, the obtained images give some indication on how adjusting the angle. After successive iterations, the IR beam should exit out of the undulator. This will provide a rough alignment of the IR laser, since the vacuum chamber of the undulators will already roughly define the axis. The undulator presents an internal gap of about 8 mm in vertical and 13 mm in horizontal.

Second, the interaction axis is better defined by using the undulator emission. The spontaneous emission of the undulator (set up in the visible or in an appropriate wavelength according to the optical performances) is auto-collimated back towards the infra-red source, ideally back to the laser hutch. The wavelength is chosen in order to have an easy observation (so that one can clearly distinguish separation between the rings) and to send back the maximum amount of light via the mirrors at 160 nm. The wavelength is selected with proper values of the undulator gap and the electron beam energy. More precisely, at the exit of the undulators, the different rings or the analysis of the spontaneous emission spectrum versus the observation position provides a very precise definition of the center of the emitted radiation, and consequently, of the axis of the electrons. Two iris are then located along this axis and then, the planar mirror used to refold the radiation in the undulator is installed at several meters from the second iris upstream of the undulators. Its transverse position is adjusted in order to send back the light in the two iris, starting from the closest iris. Then, the spontaneous emission is sent back along the axis defining the undulator axis. The light should counter propagate back in the undulator.

In a third step, the IR laser is switched on again and the two periscope mirrors are further adjusted so that the IR light should be well on the axis defined by the spontaneous emission of the undulator radiation. Then, the IR light is hidden again, and the visible emission should come back along the optics on the IR laser table. One should look on the spontaneous emission image there, and vary the diameter of the iris which is located close to the undulator exit. One should see a diffraction pattern, with different rings. If one changes de iris aperture, one should see the diffraction pattern evolving (see Fig. 37). One might be obliged to install a sensitive detector (photodiode, photomultiplier) if the image can not be seen by eye.

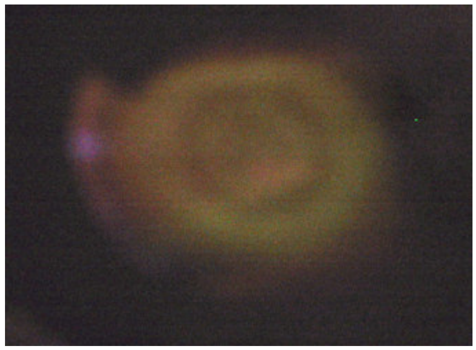

Fig. 37. *diffraction pattern of the auto-collimated spontaneous emission of the UVSOR undulator during the FEL alignment procedure. In this case, there are no intermediate optics*

If such an image is not perfectly aligned with the IR laser axis, it means that the alignment of the IR light along the two iris at the exit of the undulator is not very precise, and one should re-iterate with the adjustment of the four VUV mirrors and check the output at the exit of the undulator.

One could install a reference alignment laser going at the exit of the undulator, aligned in the two iris defining the undulator axis. This could be used as a reference and would allow the alignment to be checked regularly without redoing the whole procedure of auto-collimation.

6. The laser system

6.1. Introduction

The laser for the seeding experiment at SPARC must be integrated in the laser system that produces the photo-electrons in the injector **Errore. L'origine riferimento non è stata trovata.** . The energy per pulse of the seed signal, must be sufficient for the non-linear harmonic generation in gas at UV-VUV wavelengths. As pointed out in the previous section the required intensity for an efficient conversion in the high order harmonics in gas is of the order of 10^{14} W/cm^2. Once this value of intensity is reached, an increase in the UV power may still be obtained by increasing the laser cross section in the interaction region. For this reason an increase in the laser pulse energy provides an increase on the number of photons in the harmonics, which is the parameter that is fundamental for the success of the experiments. An energy per pulse of 2.5 mJ in the infrared is considered sufficient with a pulse duration of 100fs. Furthermore the laser pulse must be characterized by a good stability and a good transverse profile, factors that are also related to the conversion efficiency, especially of the high order harmonics. The amplifier must operate with a stretcher compressor configuration suited for this pulse duration, but at the same time we have to foresee the possibility of feeding the amplifier with a different oscillator synchronized with the main oscillator, producing shorter pulses, in the range 30-40ps, which allows the generation of harmonics of higher order for future seeding experiments. In the following we will briefly describe the RF-GUN laser system which delivers the radiation to the cathode in order, then we will define how we can interface a second laser system to provide a seed signal which has the desired properties for generating the higher order harmonics, and which is at the same time synchronized with the electrons at the undulator.

6.2. A brief description of the RF-GUN laser system

Laser to drive the photocathodes for high brightness electron beam applications must show very specific capabilities driven by two major considerations: the low photo-emission efficiency for robust photocathodes requires high UV pulse energy; the emittance compensation process is most successful with uniform temporal and spatial laser energy distribution. More demands are placed on the longitudinal (time) laser profile by the requested capability of changing the pulse length over a range from 2 to 12 ps to control the charge and peak current. Additionally, low amplitude and time jitters from pulse-to-pulse, as well as pointing stability are needed to assure repeatable SASE-FEL performance. The laser pulses have to be synchronized with the radio frequency master oscillator, in order to extract electrons at the specified phase of the RF accelerating wave. The requested features restrict the choice for the source at the solid state amplified laser based on Ti:SA active medium.

The photocathode drive laser's performance have been defined starting from beam dynamics simulations with the aim to verify as non ideal pulse features influence the electron beam's properties. In the following we describe the laser's technical feature to meet the requested performances. The laser chosen is a commercially available system. Anyway it should be noted that an external device, that in the following is named as pulse shaper, is needed to achieve the required temporal laser distribution. The drive laser supplies photons that are absorbed by electrons within the RF gun cathode, producing via the photo-electric effect emitted electrons if the energy of the photons exceeds the photocathode's work function. The energy required derives from quantum efficiency (QE). The emission threshold for metallic photocathode is generally between 4.2 and 4.6 eV, and therefore a UV light is required. Usually, from practical considerations the photon energy is set at 4.66 eV with wavelength of 266 nm. This wavelength can be produced by non-linear optical phenomena using harmonics generation in crystals. In the SPARC photo-injector the nominal charge is 1 nC, and therefore assuming a QE of ~10^{-5} for the copper cathode the required energy is 500 μJ. This required value at the photocathode, must be considerably larger at the harmonic-generator's exit, as portion of the light will be absorbed by various optical elements needed for pulse transport an manipulation to the photocathode. Beside the harmonics generator has typically efficiency on the order of 15 %, therefore the energy requirement in the fundamental harmonic is in the tens of mJ range. The QE value assumed is less than the data reported in the literature but in the energy budget we preferred to over-specify the laser performances. The energy jitters from pulse to pulse should be avoided because they induce charge and, therefore, space-charge variations and change the matching conditions. To achieve reproducible SASE-FEL performances the energy jitter has to be limited at less than 5% rms. The SPARC photo-injector repetition rate is 10 Hz and sets the laser's repetition rate.

According to theory and the simulations, the emittance compensation scheme requires a laser pulse with transverse and longitudinal profiles that are as uniform as possible. Additional demands are placed on the longitudinal (time) laser profile by the demand for the capability of changing the pulse length over a range from 2 to 12 ps to control the peak current. The correlation between the emittance performance and the variation from ideal parameter, such as energy jitters, elliptical laser spot on cathode, time jitters, were also studied with the aid of simulation codes. The working point was set at 1 nC, 35˚ of the accelerating field phase, and circular 1 mm radius spot on cathode. In terms of amplitude jitter, the results show that the emittance growth is limited to 4% and 7% for charge variation of 5% and –5% respectively. The linear dependence between laser UV energy and extracted charge means the same value for the pulse-to-pulse UV energy jitter tolerance. Simulations on timing jitter have demonstrated that the emittance variations are 4% for 1 ps time jitter between RF phase and laser pulse. Other important operational demands are high energy and pointing stability for repeatable SASE-FEL performances. To meet the requirements for the SPARC injector the pointing jitter tolerance should to be less than 33 μm in order to guarantee electron beam trajectory errors at the 1σ level. In Tab. XVIII we summarize the requirements for the laser parameters.

Tab. XVIII. *Laser requirements on cathode*

Parameter	Requirement
Operating Wavelength	260 nm
Pulse energy on cathode	500μJ (η=10^{-5})
Energy jitter (in UV)	5 % rms
Temporal pulse shape	Uniform (30% ptp)
Transverse pulse shape	Uniform (20% ptp)
Pulse rise time (10-90%)	< 1 ps
Pulse length	2-12 ps FWHM
Repetition rate	10-20 Hz
Laser-RF jitter	< 2 ps rms
Spot diameter	Circular 1 mm radius
Pointing jitter	33 μm

The whole laser apparatus which satisfies the above requirements, has been produced by Coherent Inc. A layout of the laser system is shown in Fig. 38. It is composed by the following subsystem:

1 - The "MIRA" oscillator. This is the Ti:Sa (Ti:Al2O3) oscillator which supply IR (800nn) pluses with 1,2 W of average power at a repetition rate of 79,3 MHz; this frequencies was chosen to correspond to the 36th sub-harmonic of the S-band accelerating system. The oscillator is capable to produce 100 fs pulse width with 10 nm FWHM spectra.

2 - The "HYDRA" is the amplifying apparatus which is made of all the components required for the chirp amplification process (CPA) and will be explained in what follows. The outgoing pulses have an energy of 50mJ at a repetition rate of 10Hz and is possible to achieve at maximum 70 mJ.

3 - The SHG (Second Harmonic Generation) and THG (Third Harmonic Generation) stages: here the "H" polarized amplified pulses go through two BBO crystals which are cut for phase-matching of type 1 and are 1mm thick. The pulses are transformed first in Blue light with "V" polarization at (400 nm) and then in UV pulses light at (266 nm) with "H" polarization. The outgoing pulses have an energy of about 8mJ which is the maximum efficiency for THG (~15%). The operating temperature for the crystals is the room temperature and they are protected for humidity degradation. The harmonic package is purged by nitrogen flux, so it's possible to limit the humidity of the air.

4 - The UV Stretcher stage. This is to let us have a more range of manipulation of the pulses' temporal length. In this way we are able to optimize the flat-top temporal profile of the pulses as required to minimize the transverse emittance. With this stretcher we can achieve a pulse length ranging between 1ps to 12 ps. The stretcher is based on a UV grating and therefore it introduces energy losses due to the higher diffraction orders.

The "MIRA" is pumped from a frequency doubled CW 5W diode pumped Nd:YVO_4. Being a Ti:Sa Kerr lenses mode-locked laser it supplies pulses with a large bandwidth which is indispensable to achieve the best work efficiency from the device which will allow us to modify the pulses from their Gaussian shape to the flat-top profile, that is the acousto-optic dispersive filter: "DAZZLER". The outgoing pulses are Transform Limited pulses, so they have the shortest possible temporal length regarding to their bandwidth so they satisfied the transform limited condition: $\Delta\nu\Delta\tau \sim 1$.

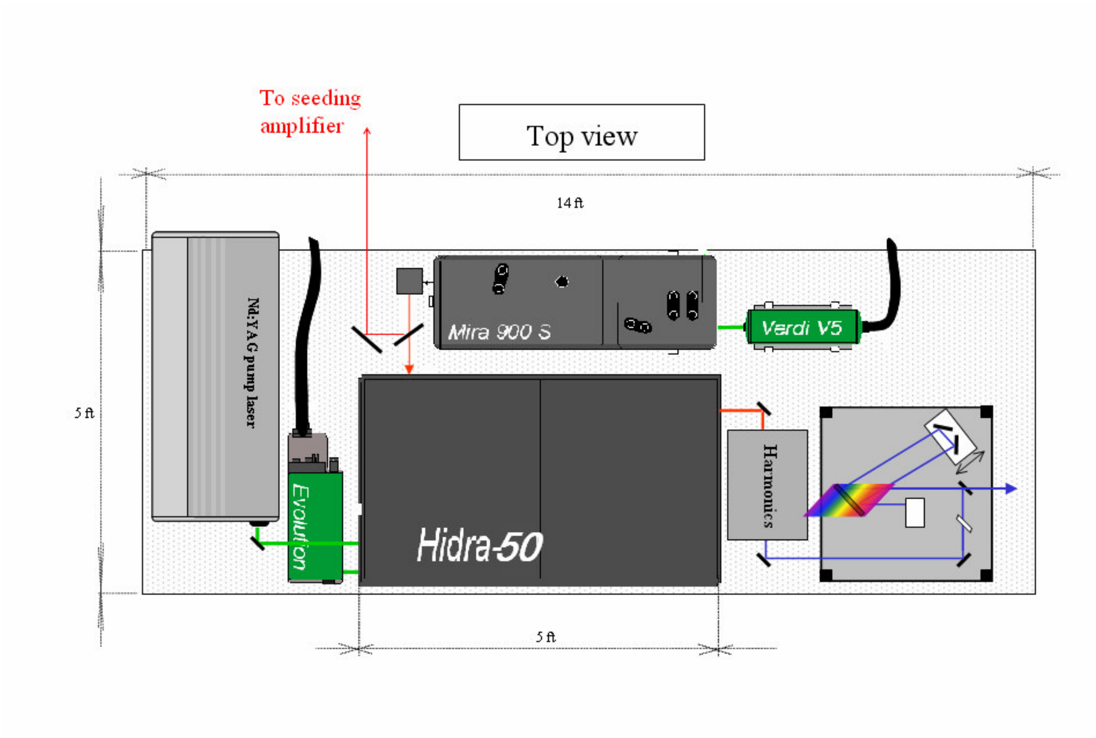

Fig. 38. *Layout of the SPARC photocathode drive laser (in red the IR portion splitted for seeding).*

Before the amplification the gaussian pulse will be spectrally manipulated to produce flat top pulse at the cathode. The 100 fs pulses delivered by the laser oscillator naturally display a Gaussian temporal profile. It is possible to manipulate the spectrum such a pulse, producing in the frequency domain f a sin(2πTf)/f function that corresponds to the required flat-top (square wave) time-profile with duration T. The devices performing this manipulation typically have high insertion losses and low damage thresholds: therefore this pulse manipulation, as well as the whole laser pulse shaping procedure, has to be applied before amplifying the laser pulse in the amplifier chain (regenerative + multi-pass).

In order to minimize any interference between the generation of the pulses between the RF-GUN drive signal and the seeding signal, it has been decided to extract the seed radiation after the MIRA oscillator, and before any temporal manipulation of the pulses. In Fig. 38 it is shown the approximate position where the IR seed extracted to drive the laser system devoted to the seeding experiment must be taken (in red). In Fig. 39 a plot of the transverse beam profile at the exit of the oscillator, is shown. This optical beam must be matched to a second amplifier chain that brings this low energy signal of 100 fs duration to the energy required for the generation of high order harmonics in gas.

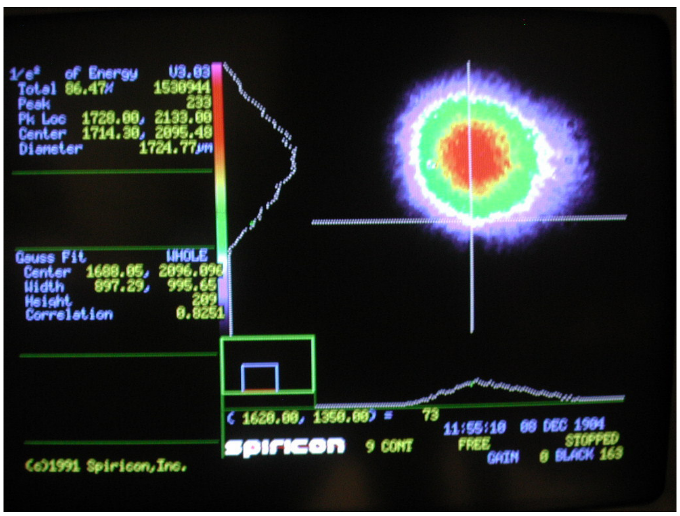

Fig. 39. *Transverse intensity distribution at the oscillator output*

6.3. The laser system for hhg generation

The energy requirement for the generation of harmonics in gas for the SPARC experiment can be fulfilled with a Ti:Sa regenerative amplifier. This class of amplifiers may deliver up to 2.5 mJ per pulse with a good transverse mode profile. The alternative is a system based on a lower intensity regenerative amplifier (1mJ) and a multipass amplifier. This scheme has the following drawbacks:

- Higher costs (two laser systems and two pump lasers)
- Higher sensitivity to alignements and more tuning requirements (note that this system is installed in a radiation exposed area and all the system must be remotely controlled)
- Lower energy stability
- Lower quality of the transverse optical profile

These aspects are particularly relevant for the SPARC experiment and for this reason the choice is in favour of a single regenerative amplifier. The compatibility with the oscillator MIRA 900-F which starts the laser chain driving the cathode suggest the model

- Coherent – Legend – F – HE

Which has an energy per pulse of 2.5 mJ (the highest value available on the market) and which may be upgraded to the model *Legend – USP – HE* which is designed to operate with pulses shorter that 50 fs.

6.4. Conversion efficiency via harmonic generation in crystal

To obtain shorter wavelengths one or two non-linear crystal (NLC) can be used. The first crystal is used as a frequency doubler and the second can be designed to produce the third or the fourth harmonic. The efficiency of conversion is proportional to the crystal length and to the power density of the input pulse. For a laser pulse of tens of femtoseconds of duration, the large bandwidth used to carry out the seeding experiment, limits the efficiency of the harmonic conversion. In fact the bandwidth a non-linear crystal can allocate is inversely proportional to its thickness and it should not be longer than 1 mm for the seeding experiment. In general the efficiency measured for the second harmonics and the second conversion is about 40 % for each stage using 1 mm BBO crystals. Therefore starting with 2.5 mJ at the fundamental wavelength we expect to obtain 1 mJ at 400 nm central wavelength and 400 μJ at 266 nm. It is clear that further losses are introduced by the optical transport to the laser-electron beam interaction region. A summary of the expected parameters is listed in Tab. XIX. The peak power is higher than the SPARC FEL saturation intensity at these wavelength. This fact ensures the possibility to seed the

Tab. XIX. *Expected parameters of the seed radiation at 400 and 266 nm generated in NLC*

Wavelength (nm)	Efficiency	Energy (mJ)	Power (GW)
800	1	2.5	25
400	40%	1.0	10
266	16%	0.4	4

7. Timing and synchronization

7.1. Introduction

In this section, we analyze the problem of the timing and the synchronization of the different components of the proposed Seeding@SPARC experiment. We will state the problem of seeding externally an FEL amplifier from the timing point of view and find out the general synchronization specifications needed for a proper setup of the experiment. Then we will show how we intend to satisfy these requirements and propose a diagram of the timing system.

The FEL amplifier is active only for the very short amount of time where the gain medium (the relativistic electron beam) is present, which is the beam bunch length (of the order of few ps). Therefore, the timing and synchronization issues of seeding an external pulse in the FEL amplifier are reduced to the problem of injecting the radiation pulse inside the undulator magnet *at the same time* of the electron beam.

This translates into two related but different requests on the timing system.

- To have the ability to synchronize deterministically the time of arrival of the electrons and the photons. This is possible since the electron bunch and the seed pulse are created from the same initial laser pulse and one has to adjust the electronic delays and relative path lengths in the accelerator and in the laser amplification chain respectively, to compensate for any differences.

- Control the jitter between the arrival times of the beams within some specifications. A ~ 1 ps jitter is tolerable in our case, since in the first proposed configurations of the Seeding@SPARC experiment, the electron beam is 10 ps long and has a flat top longitudinal profile, while the seed radiation very short (~ 100 fs). A schematic view of the seed timing requirements is shown in Fig. 40 for clarification. If, in future seeding experiments, one plans to use a shorter electron beam (e-beam compression schemes) where the electron current (and so the amplification gain) changes in time by a non-negligible amount on a temporal scale of 1 ps, this specification could get tighter. On the other hand, since the photoinjector itself is foreseen to have a timing jitter of ~ 1 ps between the photocathode driver laser and the radiofrequency waves that accelerate the electrons, it would require major improvements to the whole system to overcome this limitation.

In the second section, we will discuss briefly the photoinjector timing and synchronization system, because it is the base over which the timing scheme for the Seeding@SPARC experiment is being built.

In the third section, we will describe in details the electronic delays and the optical path length delay line that we intend to use to synchronize deterministically the pulses at the experimental point.

In the fourth section, we describe the diagnostics we intend to implement to tune up and monitor the injection timing in the FEL amplifier.

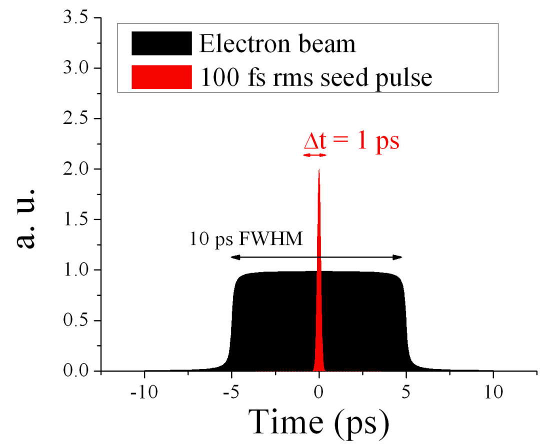

Fig. 40. *Relative timing of electrons and radiation pulse at the entrance of the FEL amplifier for Seeding@SPARC. Obviously, a 1 ps jitter is tolerable in this configuration.*

7.2. RF – Laser master oscillator synchronization

One of the main technical challenges of a photoinjector system is to synchronize the time of arrival of the laser on the cathode with the radiofrequency waves in the accelerating cavities. The longitudinal as well the transverse dynamics of the electron motion are strongly depending on the phase of the radiofrequency waves seen by the bunch in the accelerating cavities. Moreover, because of the Schottky effect at the photocathode, even the charge in the electron bunch depends on the time of arrival of the laser pulse with respect to the phase of the field in the gun.

The RF system and the laser must then be synchronized with accuracy better than 1 ps (roughly equivalent to 1 degree at 2.856 GHz) to guarantee the stability and reproducibility in all of the relevant electron beam parameters.

In addition to this very sensitive synchronization, a variety of triggers is used by the laser system, the accelerator power circuits, the diagnostics and the controls. These triggers should be synchronized with the laser and electron pulses, preceding or following them at some time-distance that depends on the device which is to be triggered. The tolerances on the timing jitter in these cases are less strict, since the events have typical time-scales much longer than the picoseconds.

In Tab. XX, we review a list of the triggers and timing signals needed for the photoinjector and their main characteristics.

Tab. XX. *List of trigger and timing signal requirements for SPARC photoinjector*

Device	**Max Jitter**	**Level**	**Frequency**
Laser oscillator (RF/36)	< 1 ps	Sinusoidal	79.3 MHz
Gun_Enable (HV modulator)	~ 1 ns		0.1 to 10 Hz
Gun_Enable (RF amplifier)	~ 1 ns	10 μs long TTL level	0.1 to 10 Hz
Evolution-15 Regenerative Pump	~ 1 ns	TTL level	1 KHz
SDGII	~ 1 ns	TTL level	Gun_Enable
Regen Pockel's Cells	~ 0.1 ns	TTL level	Gun_Enable
Nd:Yag laser lamps Double pass pump	~ 10 ns	TTL level	Gun_Enable
Nd:Yag laser lamps	~ 1 ns	TTL level	Gun_Enable

Double Q-Switch			
Oscilloscopes	~ 0.1 ns	NIM level	Gun_Enable
Digitizers	~ 0.1 ns	NIM level	Gun_Enable
Cameras	~ 100 □s	TTL level	Gun_Enable
Seed Laser Digital Delay Generators	~0.1 ns	TTL level	Gun_Enable
Streak Camera	1 ps	AC	Gun_Enable
Beam Position Monitor Front End	~ 0.1 ns		Gun_Enable
RF Feedback (RF/4)	1 ps	AC	714 MHz
RF Feedback	20 ps	NIM / ECL	Gun_Enable

Fig. 41 is a schematic that illustrates the overall electronic synchronization and timing system of the SPARC photoinjector. The blue entries are laser-internal triggers, which are transparent to the main timing system.

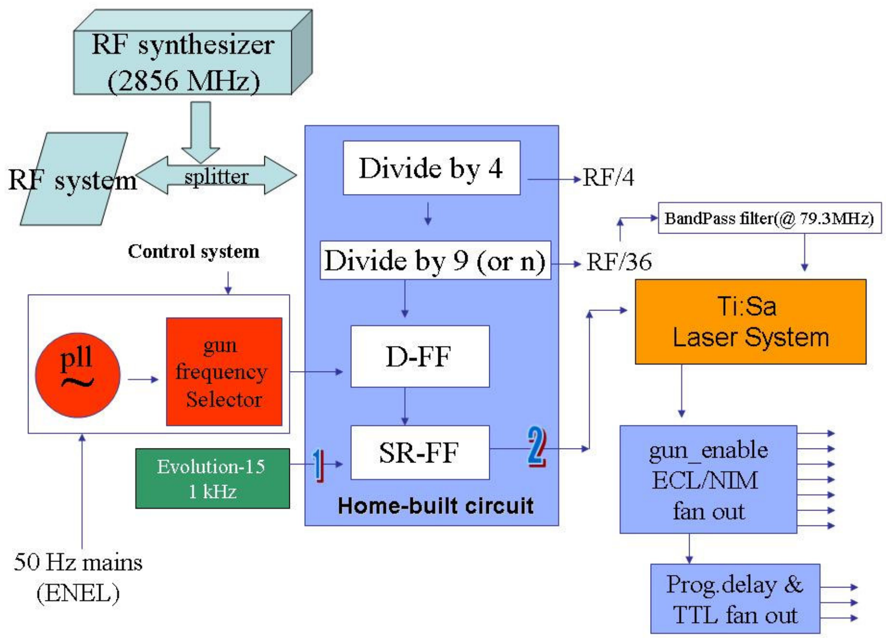

Fig. 41. *Schematics of timing system in the SPARC photoinjector.*

Let us analyze in detail the list of the electronic triggers.

A typical requirement for a particle accelerator is the locking of the repetition-rate with the line power frequency, since the ripples on the electromagnet current power supplies follow the line oscillations. Because of this, we derive by a commercial electronic device our main trigger, the gun repetition frequency (programmable in the range 0.1-10 Hz, but let us assume in the following, for sake of discussion, to be 10 Hz), locked with the 50 Hz of the line power.

This signal is sent to the home-built circuit, which receives also a 1 KHz signal coming from the laser oscillator (1 in Fig. 41 and Fig. 42). To guarantee, in fact, the gain stability in the Ti:Sa laser rods the regenerative amplifier are pumped by the Evolution-15 DPSS laser at 1 KHz repetition frequency. A home-built circuit, based on a Set-Reset flip-flop (SR-FF), selects one pulse, in the 1 KHz pulse train, that follows the 10 Hz. In this way, a rough lock to the power supply 50 Hz is accomplished (2 inFig. 41 and Fig. 42). An extra-feature of this circuit is to use a D-type flip-flop (D-FF) to synchronize the 10 Hz with the 79.3 MHz (and the 2856 MHz) for improved stability.

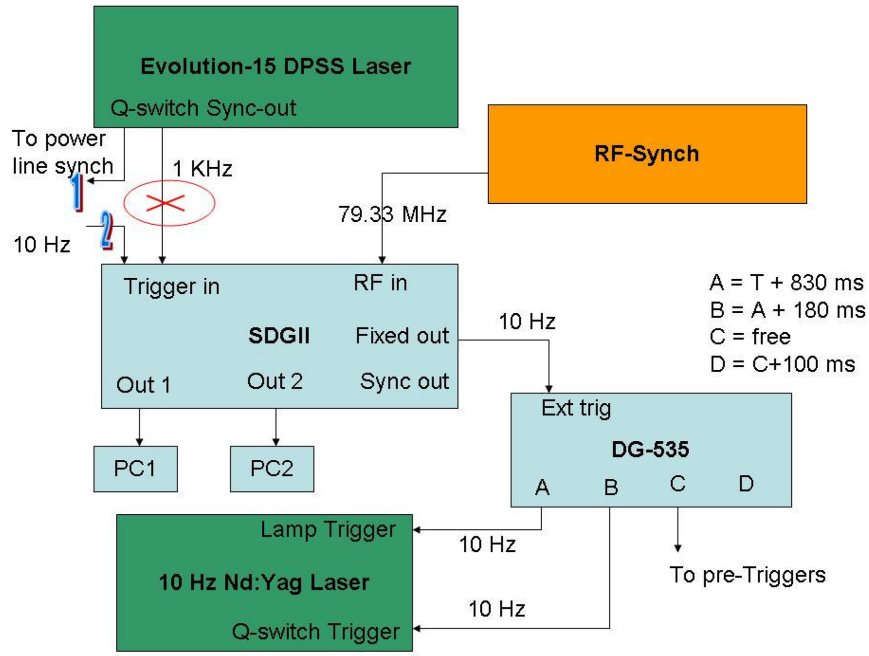

Fig. 42. *Photoinjector Driver Laser triggering system with the power line synchronization.*

The gating applied by the pulse pickers to open and close the regenerative amplifier and defines the beam-time has to be locked with the pulse train coming from the mode-locked laser oscillator in order to avoid an intra-pulse switching. This is accomplished using the laser company supplied Synchronization and Delay Generator (SDGII). The SDGII enables synchronization of a user-supplied trigger source with an external RF source (typically from the laser mode-locker). Each input trigger is precisely synchronized to the RF signal by high-speed electronics. The SDGII produces four delayed trigger signals, one fixed and three users adjustable in 250 ps steps. Two of the adjustable trigger signals are typically used to trigger the drivers of the Pockels cells in the regenerative amplifier. The other outputs are used to trigger a digital delay generator DG-535. An integrated countdown circuit conveniently allows the researcher to adjust the output repetition rate to values below the master input rate. The SDGII is microprocessor-controlled, and all delays are digitally displayed and accessible via front panel knobs, RS-232 and/or GPIB connections.

The digital delay generator triggered by the SDGII at the desired rep-rate then flashes the lamps and Q-switches the double pass amplifier laser pump. Few (10 to 20) μs before the laser pulses traverses the double pass amplifiers, it sends a trigger out of the laser system to starts the chain of the events that leads to the electron beam acceleration and diagnostics. The RF pre-amplifier is enabled to feed the klystron, the solid-state switch in the HV modulator is triggered. The DAQ oscilloscopes, the digitizers, the computers and the cameras receive also this signal and get ready for acquiring data.

The choice of a particular trigger pulse shape, level and particular timing is accomplished with the help of one or eventually more digital delay generators (Stanford Research System model DG535 with 4-channel output) located downstream of the laser DG-535. The distribution of such triggers to the users goes through NIM-ECL or TTL home-built fan outs.

Finally, we note that the jitter in the gates applied with the Pockels cells has to be small compared to the separation of the pulses in the pulse train (12 ns), but does *not* affect the path length or time of arrival of the laser pulse to the cathode. Following similar considerations, the jitter of the pump lasers triggers has to be small compared to the pumping time of the laser rods (few hundreds of ns).

The streak camera trigger on the other hand is much more sensitive to guarantee a stable picture of the fast event to be diagnosed. Usually the trigger comes from a fast photodiode conveniently located upstream arriving to the streak camera few several nanoseconds before the light.

The photodiode signal, before being available to the users, shall pass through a four-ways broadband RF splitter (passive distribution) or through an amplifier and analog fanout section (active distribution). In this way, the signal will be monitored for diagnostics purpose as well used by the RF feedback, if necessary.

7.3. Delay line for regenerative amplifier synchronizations

The previous section has described the synchronization between the photocathode driver laser and the RF accelerating waves. The seeding injection timing problem is reduced to the synchronization of two different laser systems: the photocathode driver and the infrared pulse which is used to generate the harmonics that constitute the seed the FEL amplifier.

This synchronization is made possible by using the same laser oscillator for the two laser systems. In Fig. 43 it is displayed the laser pulse distribution and timing scheme. A splitter after the oscillator sends a portion of the beam to the regenerative amplifier on the photocathode driver laser system and the other portion the transfer line to the seeding laser table.

Here the train of pulses is injected in the seeding-dedicated regenerative amplifier. The first Pockel's cell inside this device is triggered with an electronic adjustable delay which picks out one pulse in the 12 ns interval. The pulse is chosen in such a way that at the entrance of the FEL amplifier the electrons and the photons arrive with a time distance of less than 12 ns.

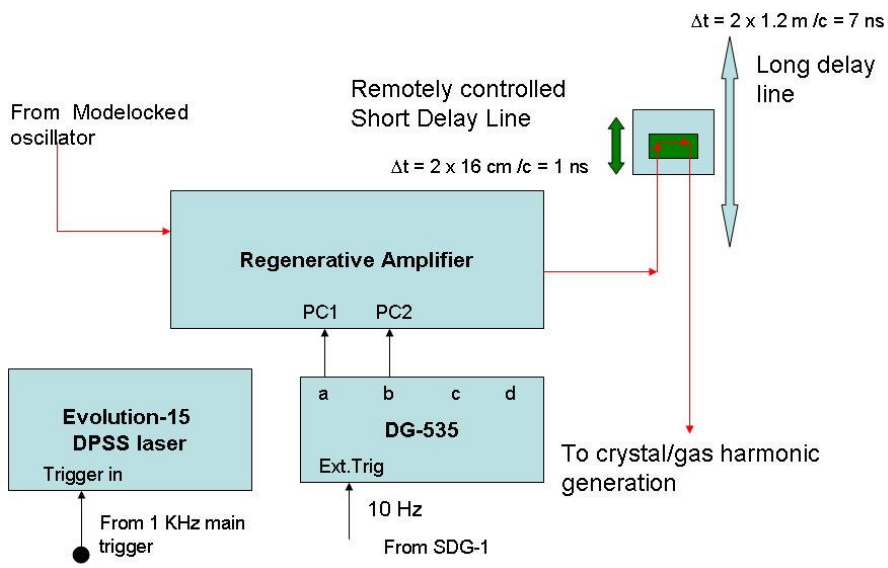

Fig. 43. *Timing scheme for the seeding laser.*

Because of stability concerns, the laser rods in the amplifier are also excited at the 1 KHz repetition rate of the pump laser. On the other hand, to facilitate the design of the vacuum system in the gas jet interaction chamber, we operate the two Pockel's cells at the gun_enable trigger rep rate (10 Hz). In such a way the seed laser fires only when the electron beam is on.

The Q-switch of the regenerative amplifier is adjusted so that the peak of the regenerative amplifier pulse train (which is now spaced by the regen cavity length ~7 ns) occurs at a time T^* that puts the electrons and the photons at the interaction region in a time interval that is less 7 ns far apart.

After the regenerative amplifier, a trombone-like optical delay line is used to synchronize the laser with the electron beams. Precise alignment of this delay line is required in order to avoid laser beam steering downstream. One portion of this delay line is motorized to do automatic scans of the timing with 100 fs resolution (~30 μm), once the ns-synchronization has been achieved electronically with the digital delay generators and then manually moving the long part of the delay line.

At this point, the laser is sent into the transfer line that leads to the interaction chamber where the higher harmonics are produced and then to the final injection mirror located on the axis of the electron beamline.

Using the Pockel's cell switching time and the delay line positions, we can always compensate any change in path length on the electron beam or the laser line. Therefore, the system, provided with a proper timing diagnostic, is always possible to be synchronized.

A similar synchronization system using one laser oscillator and two different regenerative amplifiers has already been tested and employed successfully in high power laser-electron beam interaction experiments at the Neptune Laboratory at UCLA.

7.4. Synchronization diagnostics

Time-jitters of less than a picosecond are very challenging to measure. Their deleterious effects will show up mainly on poor stability of the electron beam (when the jitter is between the photoinjector driver laser and the RF accelerating wave), and of the FEL output radiation (when the jitter is also between the two laser systems). Of course, the timing system has to provide means to check the jitter independently of the electron beam.

One possible solution is the use of a streak camera that receives the OTR light generated by the electrons and to an optical signal derived by the laser. This commercial device has usually an intrinsic accuracy of 1 ps, so it is useful to detect larger fluctuations, but, on the other hand, to achieve the best accuracy, it needs a trigger with specifications (frequency range and maximum tolerable jitter) depending by the model used.

Another possibility is by exploiting the RF frequency characteristics of the timing signals. In fact, one possibility to check single-shot time jitters is to mix the low level RF wave with a 2.856 GHz signal obtained by the signal coming from photodiode (put on the laser), or by an electron beam-related pick-up like a strip-line. The output of such mixer, accurately filtered, carries the information of the relative phase of the signals and can be used to monitor the shot-to-shot jitter with very high accuracy: this system can achieve up to 100 fs of accuracy (better than 0.1 degree of RF frequency). Limits to this approach, besides being very sensitive to the noise, could be in the intrinsic jitter of the photodiode and/or in large amplitude variations of the beam pick-up signal.

As an additional and complementary instrument devoted to the timing system diagnostics, we will use a LeCroy Wave Master 8300A oscilloscope placed in the control room. This instrument has four input channels, 3 GHz bandwidth and can acquire 20 or 10 Gsa/s. It can work in single shot and real time and therefore it can be used to monitor signals from the highest frequencies to the lowest. To monitor the correct behavior of triggers and clocks and to measure the temporal drifts that could limit the experiment performances, we will connect the following signals to the oscilloscope input channels: RF signal (2.856 GHz), laser oscillator (79.3 MHz), photodiode signal and the beam signal coming from the first pickup after the gun. Comparing the signals all together or taken as couple, we will have a flexible real-time monitor of the main temporal drifts of the accelerator. It should be noted that such scope has an intrinsic time-accuracy of ~25 ps (on the single shot). So a shot-to-shot jitter monitor is not enough precise, since the instrument jitter is much larger than the experiment needs. On the other hand, averaging over many (>30) shots, using this instrument, it is possible to monitor drifts (of the order of few ps or more) in the time-domain having time constants greater than 10-30 seconds. The same approach, applied to the comparison between RF and RF/36, will be more accurate and faster, due to the very high repetition rate of the two signals and to the jitter analysis software included in the oscilloscope.

8. Radiation Diagnostics

8.1. Spectrum

It is here presented a preliminary design of a spectrometer for the acquisition of the FEL spectral emission and intensity in the 40-550 nm region.

In this spectral interval, conventional metallic coatings (such as Au, Pt, Ir, partially Al + MgF_2) have high normal-incidence reflectivity, so the optics can be used at normal incidence, making the optical design much more simple and the performances very good. The reflectivity of some common coatings in the 40-550 nm region is shown in Fig. 44.

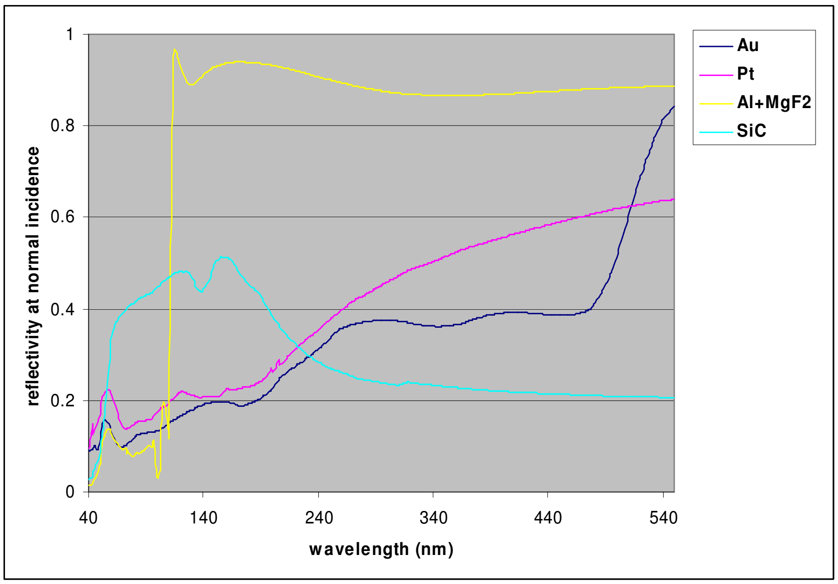

Fig. 44. *Normal-incidence reflectivity of common coatings in the 40-550 nm region.*

The main characteristics of the spectrometer are:

- It has to provide high spectral resolution ($\Delta\lambda/\lambda > 2000$)
- It has to be absolutely calibrated, in order to measure the number of emitted photons
- It has to have a large acceptance angle, to guarantee an easy alignment

The design consists of a normal-incidence spectrometer with constant subtended angle and a spherical grating which gives a spectrum on a flat detector. The spectral interval to be acquired is selected by the grating rotation. A schematic drawing is shown in Fig. 45.

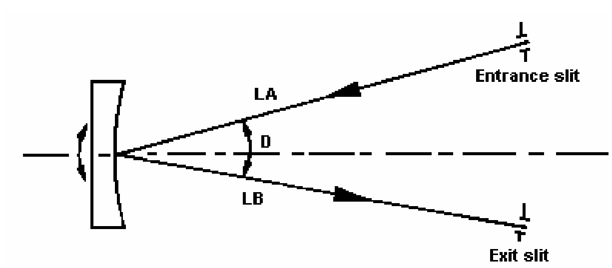

Fig. 45. *Normal-incidence monochromator.*

The source is imaged by an external optics (that in the case of the FEL radiation could be a concave mirror) on the entrance slit plane, then the concave grating provides a spectral image on the exit slit plane. In the case of a spherical grating, the image of a point-like source is a line, very narrow in the plane of spectral dispersion (in order to have the maximum resolution) and long in the plane perpendicular to the dispersion plane, because of the grating astigmatism. The latter can be corrected by a toroidal grating, obviously with higher costs. In the case of a monochromator, only the wavelength λ obeying to the grating equation $\sin(\alpha)+\sin(\beta) = m\lambda\sigma$ is transmitted from the exit slit (α and β are the incidence and diffraction angle respectively, m is the diffracted order and σ is the groove density). In the case of a spectrometer, the exit slit is substituted by a 2-D detector which acquires a spectrum in a finite interval. The portion of the spectrum to be acquired with the detector is selected by rotating the grating to change the wavelength imaged in the detector center and translating the detector along a straight line coincident with the exit arm LB to find the best focal position. The spectrometer has the characteristics listed in Tab. XXI

Tab. XXI. *Main characteristics of the spectrometer for SPARC*

entrance slit	fine regulation from 0 to 0.2 mm maximum aperture 2 mm
subtended angle	20 deg
entrance/exit arm	~980 mm
grating groove density	2400 gr/mm for the 40-180 nm region 1200 gr/mm for the 150-350 nm region 600 gr/mm for the 200-550 nm region
grating radius	1000 mm
dispersion	0.42 nm/mm (2400 gr/mm) 0.85 nm/mm (1200 gr/mm) 1.7 nm/mm (600 gr/mm)

The detector available at LUXOR is an UV-enhanced back-illuminated CCD with format 1340 × 1340 pixel and 20 μm pixel size. With such a detector, the expected performances are listed in Tab. XXII

Tab. XXII. *Spectrometer performances*

Spectral dispersion	0.008 nm/pixel (2400 gr/mm) 0.017 nm/pixel (1200 gr/mm) 0.034 nm/pixel (600 gr/mm)
Spectral interval on the CCD	11.4 nm (2400 gr/mm) 22.8 nm (1200 gr/mm) 45.6 nm (600 gr/mm)

The instrument is kept in high vacuum. All the mechanisms (slit, grating rotation, detector translation) are remotely controlled. When measuring the harmonic signal in the UV and EUV, suitable filters for the visible have to be inserted, in order to reduce the unwanted visible scattered light.

The instrument can be also absolutely calibrated in order to measure the photon flux. LUXOR has the capability of providing both the grating and filter calibration curve [53] and the detector efficiency [55]. In this case, the entrance slit is kept completely open (2 mm) to transmit the whole beam inside the instrument. The measurement of the integral spectrum gives the number of incoming photons.

8.2. Pulse duration

The temporal characterization of UV pulses emerging from the seeded system must take into account the properties of the light source. Owing to the low repetition rate, single-shot techniques should be preferred; a single-shot measurement provides also information about the reproducibility of UV pulses, like the amount of pulse-to-pulse fluctuations in energy and duration. On the other hand, single-shot measurements require high S/N ratios, which are not always achievable. Thus the measurement apparatus should be also easily convertible to a multi-shot scheme, which has less stringent requirements.

Whenever the UV pulse energy is larger than ~1μJ, autocorrelation measurements should be preferred. As a matter of fact, the use of cross-correlation techniques between IR pulses from the Ti:Sapphire driving laser and UV pulses from the seeded system are less stringent in terms of UV energy; nevertheless, optical cross-correlation measurements are not suitable for the characterization of UV pulses shorter than the IR ones. In the following we propose an autocorrelation scheme suitable for UV pulses in the 120-400 nm wavelength range. In this scheme, the pulse third-order autocorrelation is obtained exploiting the ultrafast birefringence induced in a nonlinear medium by the UV pulse itself [56]. As shown in Fig. 46, the beam emerging from the source is split by a standard UV beam splitter BS in two arms; both the beams are focused in the nonlinear medium NM by the lens *L*.

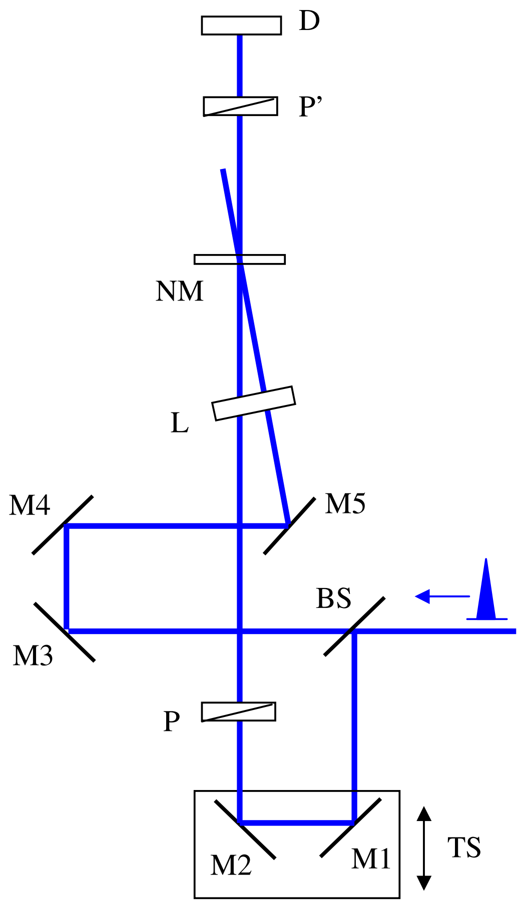

Fig. 46. *Autocorrelation scheme; BS: beam-splitter; M1-M5: mirrors; TS: translation stage; P, P': polarizers; L: lens; NM: nonlinear medium; D: detector.*

A typical nonlinear medium could be MgF_2, which shows a transparency range between 120 nm and 7 μm; the same material could be used for the lens L. For pulses shorter than 50 fs, the lens must be replaced by a focusing mirror, in order to avoid pulse lengthening due to material dispersion. The arrival time delay between the two pulses can be finely adjusted using the translation stage TS. The polarizer P imposes on the first beam a polarization direction making a 45° angle with respect to the second beam; polarizers made of α-BBO can be used in the UV down to 190 nm; the polarizar P could be also replaced by a suitably designed half-wave plate. Owing to the interaction between the two beams in the nonlinear medium NM, the polarization state of the first beam will change; this change will be detected using the polarizer-analyser P' in front of the detector D. It is worth noting that the polarization state of the first beam changes only when the two pulses are overlapping in time and space inside the medium NM, thus allowing the detection of the autocorrelation signal as a function of the delay between the two pulses.

In a multi-shot configuration, the autocorrelation is recorded by changing the delay through the translation stage TS; in this case the two beams are focused in the medium NM by a spherical lens (or a spherical mirror for few-femtosecond pulses); the signal detection is then achieved using a photodiode or a photomultiplier.

The single-shot configuration is obtained fixing the position of the translation stage TS, replacing the spherical lens (mirror) with a cylindrical one and using a detector array instead of a single detector. Let assume that t and τ are the arrival time in the nonlinear medium of the first and the second pulse respectively; owing to the macroscopic dimension of the two beams (indeed the cylindrical lens focuses the two beams only in one dimension), the delay T = τ - t between the pulses changes with the position along the medium, as shown in Fig. 47. It can be easily verified that T is related to the position x along the medium by the expression

$$\mathrm{T} = \frac{x}{c}\,\mathrm{sen}(\alpha) \tag{18}$$

where c is the light speed and α is the angle between the propagation directions of the two beams.

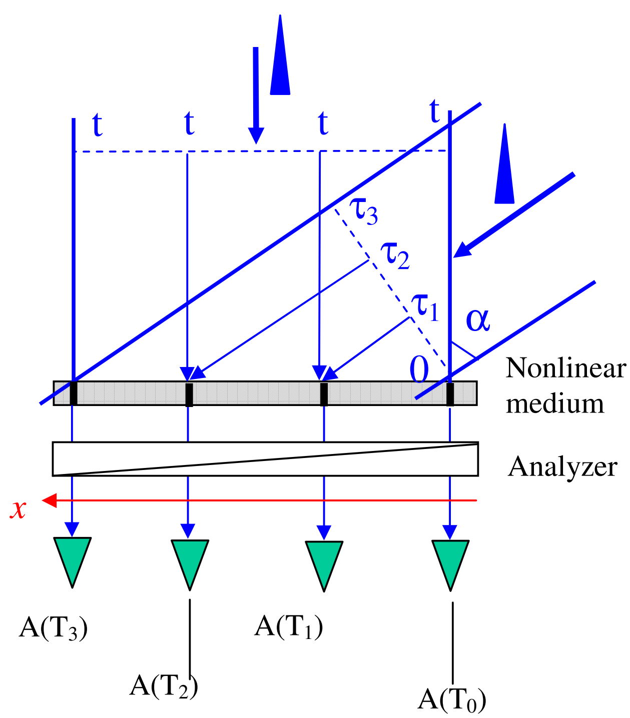

Fig. 47. *Single-shot interaction between the UV pulses*

Thus the autocorrelation A(T) can be measured using a detector array in front of the analyser P' and translating the measured signal from the spatial to the temporal domain using the previous relation. For a detector array with a pixel dimension of 20 μm, one can obtain a temporal resolution in the autocorrelation of about 1 fs using an angle $\alpha \cong 1°$ between the two beams.

9. References

[1] L.H. Yu, Phys. Rev. A, 44, 5178 (1991)
[2] F. Ciocci et al, IEEE Jour. Quant. Elec. 31 (7) (1995) 1242-1252
[3] L. H. Yu, I. Ben-Zvi, Nucl. Inst. Meth. A393 (1997) 96
[4] S. G. Biedron et al., Nucl. Inst. Meth. A475 (2001) 401
[5] R. Barbini et al., in Proceedings of Prospects for a 1A FEL Laser, Sag Harbor, New York, 1990, edited by J. Gallardo (BNL Report No. 52273, 1990)
[6] DESY Report No. TDR-2001-23, 2001
[7] 4GLS: http://www.4gls.ac.uk/
[8] ARC-EN-CIEL "Une installation innovante de source de quatrième génération": http://lure.u-psud.fr/congres/femto/
[9] BESSY : http://www.bessy.de/front_content.php?idcat=31
[10] DESY: http://www-hasylab.desy.de/facility/fel/main.htm
[11] FERMI: http://www.elettra.trieste.it/projects/fermi_public/
[12] MAX-4: http://www.maxlab.lu.se/acc-phys/projects/max4/index.htm
[13] SPARX: http://www.sparx.it
[14] An overview of existing and proposed FEL sources with hyperlinks is available at http://www-hasylab.desy.de/facility/fel/overview/fel_laboratories.htm
[15] H.P. Freund, P. G. O'Shea NIM A483, 449 (2002)
[16] W.M. Fawley, W.A. Barletta, J.N. Corlett, and A. Zholents, Simulation Studies of a Xuv/Soft X-Ray Harmonic-Cascade fel For The proposed LBNL recirculating Linac, in proceedings of PAC 03
[17] MIT-BATES proposal: http://mitbates.mit.edu/xfel/
[18] K. Midorikawa, Phys rev Let 82 1422 (1999)
[19] D. Garzella et al., NIM A 528, 502 (2004)
[20] P. Zeitoun et al, Second generation X-ray laser, NATURE to be published
[21] E.L. Saldin, E. A. Schneidmiller, M.V. Yurkov, Optics Comm. 202, (2002) 169
[22] L. Giannessi, P. Musumeci, S. Spampanati, *Non-linear pulse evolution in seeded and cascaded free electron lasers*, submitted to J. of Appl. Phys, March 2005
[23] SPARC Collaboration, Nucl. Instr. & Meth. A507 (2003) 345-349, see also http://www.sparc.it
[24] I. A. Walmsley, Optics & Photonics News, April 1999, p.28
[25] I. Ben Zvi, K. M. Yang, and L. H. Yu, NIM A 318, 726 (1992).
[26] F. Ciocci et. Al., *Proposition of Experiment at SPARC: Harmonic Generation Seeded by High Order Harminics Produces in Gas Sparc Tech note* SPARC-FEL-04/005 available at http://www.sparc.it/
[27] Sparc Injector TDR – http://www.lnf.infn.it/acceleratori/sparc/SPARC_TDR.pdf
[28] R. Bonifacio, N. Piovella, and B. W. J. McNeil, Physical Review A 44, R3441 (1991).
[29] "LCLS Conceptual Design Report", SLAC-R-593, april 2002,UC-414, pag. 7-73
[30] P. B. Corkum, Phys. Rev. Lett. 71 (1993) 1994-1997.
[31] M. Lewenstein et al., Phys. Rev. A 49 (1994) 2117.
[32] H. Eichmann et al., Phys. Rev. A 51 (1995) R3414
[33] P. Salières et al, Adv. At., Mol., Opt. Phys. 41 (1999) 83.
[34] P. Salières et al., Science 292 (2001) 902
[35] L. Le Déroff et al., Phys. Rev. A 61 (2000) 043802.
[36] Takahashi et al., JOSA B 20, 158 (2003)
[37] Takahashi et al., Opt. Lett. 27, 1920–1922 (2002)
[38] Takahashi et al., Phys. Rev. A 66 021802 R (2002)
[39] Takahashi et al., Techn. Digest, 10th Int. Conf High Field and Short wavelength Sources, Oct 12-15, 2003, Biarritz, p. 319.

[40] Hergott et al., PRA 66, 021801 (2002)
[41] Kazamias, Ph.D. thesis, Orsay (2003)
[42] Dolle et al., Appl. Phys. B 75, 629 (2002)
[43] F. Ciocci et. Al., *SPARC Undulator Parameter Set* SPARC-FEL-03/003 available at http://www.sparc.it/
[44] L. Giannessi et. Al., *SPARC Transfer Line* SPARC-FEL-03/006 available at http://www.sparc.it/
[45] K. Bane and M. Sands, "Wakefields of very short bunches in an accelerating cavity", in Proc. Workshop on Impedances Beyond Cut-off, 1987, 1987.
[46] L. Palumbo, V. G. Vaccaro, and M. Zobov, "Wake fields and impedance", Proc. CERN Accelerator School: Advanced Accelerator Physics Course, Rhodes, 1993, n. 95-06.
[47] H. Chin, "Advances and applications of ABCI", LBL-33268, ESG-220, presented at the 1993 Particle Accelerator Conference, Washington, DC, May 17-20, 1993.
[48] R. Klatt, et al., "MAFIA—a three dimensional electromagnetic CAD system for magnets, RF structures and transient wake-field calculations", Proceedings of the 1986 Linear Accelerator Conference, SLAC-Report 303, June 1986, pp. 276–278.
[49] H. Merdji, private communication.
[50] L. Giannessi, presentation at http://www.frascati.enea.it/SPARCWORKSHOP/programma.htm
[51] H. Merdji, Jobin-Yvon, private communication
[52] D. Nutarelli, Thèse de doctorat
[53] Sparc Injector TDR, *Photocathode Drive Laser System,* p.78 – http://www.lnf.infn.it/acceleratori/sparc/SPARC_TDR.pdf
[54] L. Poletto et al, Opt. Eng. 40, 178, 2001
[55] L. Poletto et al, Appl. Opt. 38, 30, 1999
[56] H.-S. Albrecht, P. Heist, J. Kleinschmidt, D. V. Lap, T. chr Soder, Appl. Opt. 32, 6659 (1993).